HNRNP E1 PROTECTS CHROMOSOMAL STABILITY THROUGH POST-TRANSCRIPTIONAL REGULATION OF CDC27 EXPRESSION

A dissertation submitted

to Kent State University in partial

fulfillment of the requirements for the

degree of Doctor of Philosophy

by

Laura Link Schwartz

December 2015

Dissertation written by

Laura Link Schwartz

B.S., University of Toledo, 2010

Ph.D., Kent State University, 2015

Approved by

Philip H. Howe, Ph.D., Chair, Department of Biochemistry (MUSC), Doctoral Advisor

Derek S. Damron, Ph.D., Professor, Department of Biological Sciences

Gail C. Fraizer, Ph.D., Associate Professor, Department of Biological Sciences

Sean L. Veney, Ph.D., Associate Professor, Department of Biological Sciences

Roger B. Gregory, Ph.D., Professor, Department of Chemistry

Accepted by

Ernest J. Freeman, Ph.D., Director, School of Biomedical Sciences

James L. Blank, Ph.D., Dean, College of Arts and Sciences

List of Figures

List of Tables

List of Abbreviations

APC/C: anaphase-promoting complex/cyclosome E3 ubiquitin ligase

APC3: anaphase-promoting complex subunit 3

ß-TRCP: beta-transducing repeat-containing protein

Cdc20: cell division cycle 20

Cdc27: cell division cycle 27

Cdh1: cell division cycle 20-homolog 1

EMT: epithelial-to-mesenchymal transition

Fzr1: fizzy/cell division cycle 20 related 1

MCC: mitotic checkpoint complex

Pak1: p21-activated kinase 1

Plk1: polo-like kinase 1

SCF: Skp1-Cullin-F Box E3 ubiquitin ligase

Skp2: S-phase kinase-associated protein 2

TGFß: transforming growth factor beta

NMuMG: Normal murine mammary gland cells

NMuMG-Cdc27: NMuMGs transfected with Flag-tagged Cdc27 ORF

E1KD: NMuMG-hnRNP E1-knockdown cells

M1P: Primary mammary tumor cell line from E1KD-injected NOD/SCID mouse

L1P: Cell line generated from lung metastases of E1KD-injected NOD/SCID mouse

L2P: Cell line generated from lung metastases of L1P-injected NOD/SCID mouse

Dedication

I would like to dedicate this dissertation:

to my parents, Jeff and Sharon,

for their love and support;

and to my loving husband, Peter,

for his endless patience and encouragement.

Preface

The *in vivo* progression series project presented in this dissertation was done in collaboration with Dr. Breege Howley. The invasion, migration, and lung colonization assay data presented in Figure 19 have been published (Howley, Hussey, Link, & Howe, 2015).

Acknowledgements

I would like to express my sincere appreciation and gratitude to my advisor, Dr. Philip H. Howe, for his mentorship throughout this process. I am truly fortunate to have had the opportunity to work with him.

I would also like to thank my advisory committee members, Dr. Derek Damron, Dr. Gail Fraizer, and Dr. Sean Veney for their invaluable guidance, feedback, and especially their flexibility in working with a student from several states away.

Finally, I would like to express my thanks to members of my lab for their critical insight and collaboration, especially Dr. Breege Howley.

Laura Schwartz

August 16, 2015

Charleston, South Carolina

I. Chapter 1: Introduction

When breast cancer progression reaches its final metastatic stage, the disease is considered incurable. While considerable advances have been made in early detection, it is now believed that metastasis is an earlier step in tumor development than previously thought, thereby making it very difficult to prevent (Balic et al., 2006; Dumont et al., 2013). Furthermore, much remains unknown about the mechanisms that underlie metastasis. In the past, whole genome microarray analysis has been utilized to interrogate patient tumor samples to identify transcriptional changes that occur as cells undergo tumorigenic and metastatic progression in an effort to identify novel disease biomarkers. However, this approach has yielded limited success, likely because the transcriptome does not accurately mirror the proteome. There are several layers of regulation that play a role in determining whether an mRNA transcript is translated into protein. Heterogeneous ribonucleoprotein E1 (HnRNP E1) is an RNA-binding protein that is known to function in regulation of mRNA splicing, transcription, and translation. Previously, we characterized the role of hnRNP E1 in translational regulation of mRNAs involved in TGFβ-mediated epithelial-to-mesenchymal transition (EMT) (Chaudhury, Hussey, et al., 2010; Hussey et al., 2011). Here, we find that hnRNP E1 regulates translation of mRNAs in a variety of other biological processes besides EMT, including cell cycle. In particular, this dissertation investigates the hnRNP E1-mediated translational regulation of expression of Cdc27, a core component of the anaphase-promoting complex/cyclosome (APC/C).

In normal cells, a tightly regulated system is in place that ensures precise duplication and division of genetic material, maintaining the genome throughout generations of cells. Deregulation of cell cycle is one of the many hallmarks of cancer and its

consequences include chromosomal instability. The APC/C is an E3 ubiquitin ligase whose primary activity is ubiquitinating substrates involved in cell cycle progression, thereby preventing premature S phase entry during G1 and promoting anaphase during mitosis. Ineffective regulation of APC/C activity results in genomic instability: cells prematurely enter S phase, resulting in DNA replication errors, or divide their DNA prior to proper alignment and attachment during metaphase. The predisposition to chromosomal aberrations is advantageous for cancer cells, as they are better able to adapt to changes in their microenvironments such as nutrient fluctuation and hypoxia during the multi-step process of metastasis. Not only does chromosomal instability favor metastasis, it also complicates the clinical treatment of the disease, as the tumors are phenotypically heterogeneous and treatment-resistant subpopulations arise. It is therefore essential to uncover the mechanisms that underlie the regulation of chromosomal stability to better understand the process of metastasis.

The purpose of this study is to investigate the contribution of hnRNP E1 to cell cycle regulation, specifically through its post-transcriptional regulation of Cdc27 expression. Cdc27 was identified in a screen of transcripts that were translationally upregulated in hnRNP E1-null cells. First, we validate the translational upregulation of Cdc27 in hnRNP E1-knockdown cells. Then, we explore hnRNP E1-mediated regulation of Cdc27 mRNA translation during the cell cycle. We proceed by identifying the kinase responsible for hnRNP E1 phosphorylation, which modulates its binding to Cdc27 mRNA. The role of constitutive expression of Cdc27 is assessed with regard to APC/C function and chromosomal instability. Finally, the relevance of Cdc27 in human breast cancer cell lines and patient samples is addressed. Based on previous results and preliminary data, we

propose that hnRNP E1 acts as a tumor suppressor and loss of its translational silencing function through increased proliferative signaling leads to aberrant expression of cell cycle proteins involved in acquisition of a pro-metastatic phenotype. The use of cultured cell lines presents limitations when studying human disease. We have attempted to reduce the effect of these limitations by repeating *in vitro* experiments in human cell lines, as well as analyzing patient samples and data. In summary, we explore the mechanisms upstream of Cdc27 translational regulation and downstream of constitutive Cdc27 expression in the context of breast cancer progression.

In our previous studies, we focused on the role of heterogeneous ribonucleoprotein E1 in TGFβ-dependent translational silencing in the process of epithelial-to-mesenchymal transition (EMT) (Chaudhury, Hussey, et al., 2010; Howley et al., 2015; Hussey et al., 2011; Hussey et al., 2012). Normal murine mammary gland cells (NMuMG) were used, as they are an established model cell line for studying TGFβ-induced EMT (Moustakas & Heldin, 2005; Zavadil & Bottinger, 2005). To generate a list of mRNAs that were translationally silenced by hnRNP E1, and then actively translated upon stimulation with TGFβ, a combinatorial method was employed using both polysome profiling and Affymetrix array analysis. Briefly, NMuMGs, NMuMGs treated with TGFβ, and NMuMGs in which hnRNP E1 had been stably silenced (E1KDs) were subject to polysome profiling followed by Affymetrix array analysis. NMuMG and E1KD cells were synchronized by culturing in low serum medium overnight. To validate the synchronization, cell cycle profiles were obtained by propidium iodide staining followed by flow cytometric analysis of total DNA content in cells. When analyzing a population of cells for cell cycle phase by propidium iodide staining, one will usually obtain two distinct peaks in a histogram with the propidium iodide staining on the x-axis.

The first peak represents the G1 population and the DNA content is said to be 2N. The second peak should correspond to a number on the x-axis that is double the number under the first G1 peak. This peak corresponds to the G2/M population and the DNA content is said to be 4N. Any cells that exhibit an intermediate DNA content between 2N and 4N are progressing through S phase.

Polysome profiling involves the sedimentation of cytosolic extracts from cells, separating the less dense fractions from the more dense fractions. When collecting fractions from the sucrose gradient after ribosome sedimentation, the absorbance is read at 254 nm. This absorbance value is then plotted on a graph versus fraction number. The absorbance corresponds to the ribosomal RNA in the sample, and allows for the assignment of monosome or polysome to fractions. The highest peak corresponds to the complete 80S ribosome, and any fractions lighter than and including the 80S are considered monosomal, and those heavier than the 80S are considered polysomal. After collecting the individual fractions, total RNA is isolated and analyzed by RNA electrophoresis to determine the identity of the fractions. Because ribosomal RNA is very abundant, it is easily detectable by agarose gel electrophoresis and ethidium bromide staining. The differential distribution of the 18S and 28S rRNA in the fractions reveals the presence of 40S, 60S, or 80S ribosomal subunits. The mRNA isolated from the dense fractions is considered actively translating, polysomal mRNA because of its association with more than one ribosome. The mRNA isolated from the light fractions is considered translationally silent or weak, as it is only present in fractions containing only 40S or 60S ribosomal translation complexes. The RNA isolated from monosomal and polysomal fractions was then transcribed into complementary DNA (cDNA) and hybridized to an

Affymetrix array chip. The cDNA synthesis and Affymetrix array analysis was performed by the Medical University of South Carolina Proteogenomics Facility.

The results of the previous Affymetrix array analysis allowed for the identification of a group of mRNAs whose translation was both TGFβ- and hnRNP E1-dependent, previously termed "BAT" genes, for TGFβ-activated translation genes (Chaudhury, Hussey, et al., 2010; Hussey et al., 2011; Hussey et al., 2012). While this study yielded many interesting TGFβ-sensitive hnRNP E1 targets of translational regulation including Dab2, ILEI, and Inhibin β-A, there were yet a large number of mRNAs that were translationally silent in NMuMGs and active in E1KDs, independent of TGFβ. Furthermore, some preliminary data with E1KD cells revealed that they were more invasive and aggressive than NMuMGs treated with TGFβ, suggesting that hnRNP E1 was regulating processes downstream of other stimuli besides TGFβ.

II. Chapter 2: Review of Literature

Assessing mRNA translation Affymetrix and microarray technologies have recently achieved popularity as methods for high-throughput screening of biological samples to analyze mRNA expression in an effort to curate disease-specific gene signatures. It was hoped that these gene signatures would aid in identifying novel disease biomarkers to facilitate patient stratification and assignment of therapeutic strategies. However, attempts to correlate mRNA expression with relative protein abundance have yielded variable results, as it became evident that the proteome did not accurately mirror the transcriptome (Ghazalpour et al., 2011; Schwanhausser et al., 2011). Post-transcriptional regulation plays a major role in the determination of the fate of messenger RNAs, so it is not surprising that specific mRNA abundance did not accurately reflect the level of protein. The methods currently available for proteomic profiling include two-dimensional gel electrophoresis and mass spectrometry, both of which are labor-intensive and require a high level of expertise. In order to better assess the relationship between mRNA expression and protein abundance, we decided to utilize polysome profiling. Polysome profile analysis provides an attractive alternative, in that it is relatively simple and inexpensive, and offers a more accurate perspective on the level of protein expression based on the efficiency with which its mRNA is being translated. Described previously by Merrick et al., this method allows for the linear separation of RNA based on its density, in direct correlation with its association with ribosomal subunits (Merrick & Hensold, 2001). Combined with Affymetrix array analysis, polysome profiling is a powerful technique that allows identification of transcripts based on their differential translational efficiency. This is a better predictor of protein expression than Affymetrix array analysis alone, but is not without limitations.

Polysome profiling does not account for post-translational modifications that affect the stability of proteins, and so must be validated by other protein-detection techniques.

Regulation of mRNA expression at the translational level offers a distinct advantage to cells: response to intra- and extracellular cues can be mediated swiftly in the presence of a pre-transcribed mRNA, without the need to first transcribe a gene. This adaptation is a valuable tool that may be exploited by cancer cells, as they have an increased need for adaptability during the multistep process of metastasis as they proceed from one locale to the next (Silvera, Formenti, & Schneider, 2010). Furthermore, translational regulation of mRNA expression is necessary during normal cellular development, as transcription does not occur immediately in the embryo and maternal mRNA translation must be regulated in a spatiotemporal manner (Kronja & Orr-Weaver, 2011). A central theme exists in translational regulation, and that is the recognition of 3' untranslated regions (UTRs) of mRNAs by RNA-binding proteins or microRNAs, whose interaction serves to repress or activate translation (Baker & Coller, 2006).

Heterogeneous ribonucleoprotein E1 and regulation of translation

Heterogeneous ribonucleoproteins represent a multifunctional family of RNA-binding proteins that form hnRNP complexes and regulate a variety of post-transcriptional RNA processes including mRNA stability and translation, as well as subcellular localization of RNA (Chaudhury, Chander, & Howe, 2010). Heterogeneous nuclear ribonucleoprotein E1 (hnRNP E1), in particular, is ubiquitously expressed and has been shown to regulate some aspects of mRNA biology including mRNA stability and translational regulation (Meng et al., 2007; Ostareck et al., 1997; Ostareck-Lederer, Ostareck, & Hentze, 1998). The mechanisms described for hnRNP E1-mRNA interaction follow the canonical architecture set forth by

other RNA-binding proteins, in that hnRNP E1 has been shown to localize to 3' UTRs of its target genes. HnRNP E1 was described in its role as a repressor of 15-lipoxygenase mRNA translation during red blood cell maturation. A regulatory motif, termed "DICE" for differentiation control element, was identified in the 3' UTR of 15-lipoxygenase mRNA, and it was shown that hnRNP E1 interacted with this element, silencing translation until late in erythropoiesis (Ostareck et al., 1997; Ostareck-Lederer, Ostareck, Standart, & Thiele, 1994). Others described the contribution of hnRNP E1 binding to the 3' UTR of α-globin mRNA, stabilizing it by attenuating deadenylation during erythrocyte production (Morales, Russell, & Liebhaber, 1997; Weiss & Liebhaber, 1994). The mechanisms by which hnRNP E1 had been shown to bind and regulate mRNA provided a scaffold upon which the TGFβ-mediated "BAT" mechanism was later modeled (Chaudhury, Hussey, et al., 2010).

Through a series of experiments, Hussey et al. identified an mRNP complex wherein hnRNP E1, along with elongation factor 1 alpha 1 (EF1A1), act as *trans* factors to silence translation by binding the 3' untranslated region (UTR) of mRNAs containing a specific *cis* regulatory element that was termed "BAT" for TGFβ-activated translation. Translational silencing conferred by hnRNP E1 could be relieved by transforming growth factor β (TGFβ) stimulation, through noncanonical activation of the PI3K signaling pathway, resulting in the Akt2-dependent phosphorylation of hnRNP E1 at its serine 43 residue. This phosphorylation event was sufficient to abrogate translational silencing of *Dab2* and *ILEI*, two EMT-inducer transcripts. The observed increase in the abundance of disabled-2 (Dab2) and interleukin-like EMT-inducer (ILEI) occurred without a concomitant increase in mRNA expression, supporting the model that the increase in expression observed was a result of

post-transcriptional gene control (Chaudhury, Hussey, et al., 2010; Hussey et al., 2011; Hussey et al., 2012).

Stable knockdown of hnRNP E1 expression in normal murine mammary gland (NMuMG) cells resulted not only in the increase in Dab2 and ILEI expression, but also in the acquisition of a mesenchymal phenotype *in vitro* characterized by a gain of mesenchymal cell markers and a loss of epithelial cell markers (Chaudhury, Hussey, et al., 2010), and *in vivo* characterized by acquisition of invasive and metastatic capabilities (Howley et al., 2015). To further investigate the scope of hnRNP E1-mediated translational control, a combinatorial approach involving differential gene expression profiling and transcriptomic analysis was utilized: Affymetrix array analysis was performed on cDNA generated from the monosomal or polysomal RNA of NMuMG and E1KD cells (Hussey et al., 2012). In brief, differential sedimentation was used to separate dense, ribosome-rich mRNA (polysome) fractions from light, ribosome-poor mRNA (monosome) fractions. RNA isolated from distinct fractions was reverse transcribed, and then the cDNA generated was subject to Affymetrix array analysis to identify genes that are constitutively expressed in the polysomal fractions of E1KDs, while they remained in the monosomal fractions of NMuMG controls. While the initial purpose of the experiment was to identify genes that were both hnRNP E1- and TGFβ-dependent, there were a large number of genes that appeared to be regulated by hnRNP E1 independent of TGFβ.

Phosphorylation of hnRNP E1 and its effect on translational silencing

Phosphorylation of heterogeneous ribonucleoproteins has been said to impact their affinity for RNA (Dreyfuss, Matunis, Pinol-Roma, & Burd, 1993). Previously, our research focused on TGFβ-induced activation of Akt2 and its phosphorylation of hnRNP E1. However, a large

number of hnRNP E1-regulated genes identified in our screen were not influenced by TGFβ, and that led us to investigate other possible upstream modulators of hnRNP E1 function. It has been previously reported by others that p21-activated kinase 1 (Pak1) can phosphorylate hnRNP E1, abrogating its binding to a 3' UTR *cis* regulatory element in L1CAM mRNA. HnRNP E1 could successfully silence *in vitro* translation of a synthetic reporter gene with the L1CAM DICE element cloned downstream (Meng et al., 2007). Because of this, Pak1 was considered early on as an alternative candidate for hnRNP E1 phosphorylation in the context of translational repression. Pak1 is normally activated by the small GTPases Cdc42 and Rac (Viaud & Peterson, 2009), however one of the hallmarks of cancer is sustained proliferative signaling without the need for exogenous growth stimuli (Hanahan & Weinberg, 2000, 2011). Furthermore, constitutive Pak1 activation is a prevalent characteristic in many types of cancer (Wang, Zhang, Balasenthil, Medina, & Kumar, 2006). Identifying downstream targets of Pak1 activation would be a valuable finding in revealing cellular pathways that are exploited by cancer cells.

Translational regulation of Cdc27 expression The goal of this research is to elucidate the extent to which hnRNP E1 is involved in cell cycle regulation through translational silencing of a subset of cell cycle-related mRNAs. Through the previously mentioned screen of hnRNP E1-regulated genes, we investigate cell division cycle 27 (Cdc27), an mRNA encoding for a core subunit of the anaphase-promoting complex/cyclosome (APC/C). HnRNP E1-mediated regulation of Cdc27 translation has not been previously reported. The APC/C is a large, multi-subunit E3 ubiquitin ligase that is responsible for ubiquitinating cell cycle proteins for proteasome-mediated degradation (Peters, 2002, 2006). The careful regulation of APC/C activity is critical in order to prevent

premature ubiquitination of substrates such as securin and cyclin B1 (Listovsky & Sale, 2013; Prosser, Samant, Baxter, Morrison, & Fry, 2012). It has been shown that premature activation of the APC/C can lead to metaphase arrest, sometimes resulting in centrosome amplification and aneuploid cell division (Eytan, Sitry-Shevah, Teichner, & Hershko, 2013; Listovsky & Sale, 2013; Prosser et al., 2012). Previous research has focused on the role of the mitotic checkpoint complex (MCC) in regulating APC/C function during mitosis (Penas, Ramachandran, & Ayad, 2011; Sudakin, Chan, & Yen, 2001; Tipton et al., 2011), wherein the MCC functions to sequester the APC/C-activating cofactor, Cdc20, prior to proper chromosome-microtubule attachment at the metaphase plate. Because of its identification as an hnRNP E1-regulated mRNA, we investigate the contribution of Cdc27 to the metastatic phenotype exhibited by hnRNP E1-knockdown cells.

Cdc27 function in APC/C and cell cycle regulation Cdc27 is one of thirteen subunits that comprise the eukaryotic anaphase promoting complex/cyclosome, a large E3 ubiquitin ligase that targets specific proteins for degradation during the cell cycle (Peters, 2002). Of the core subunits, Cdc27 is unique in that it directly associates with either of two cofactors that govern the specificity of the APC/C ubiquitin ligase, Cdh1 or Cdc20. The APC/C^{Cdh1} is active during late mitosis through G1 phase, whereas the APC/C^{Cdc20} is active only during anaphase. The APC/C^{Cdc20} is normally inhibited until the cell senses that sister chromatids are properly aligned at the metaphase plate and all kinetochores are attached to microtubules of the mitotic spindle. Only then is the APC/C^{Cdc20} activated and securin and cyclin B are degraded, allowing for the metaphase-to-anaphase transition and for the genetic material of the cell to be divided evenly (Kramer, Scheuringer, Podtelejnikov, Mann, & Peters, 2000; Peters, 2002, 2006). The mitotic checkpoint complex (MCC) is responsible

for inhibiting APC^{Cdc20} activity by sequestering Cdc20 during mitosis until bipolar spindle attachment has been achieved (Sudakin et al., 2001; Tipton et al., 2011). Here we investigate the consequences of constitutive expression of Cdc27 resulting from loss of hnRNP E1-mediated translational silencing.

Previously, others have investigated the expression of Cdc27 in breast cancer. Pawar et al. concluded that Cdc27 might act as a tumor suppressor by inducing APC/C-dependent degradation of Cyclin D1. They report that the transcription factor, CEBPδ, is responsible for increased *Cdc27* transcription in mouse embryonic fibroblasts, and that this increase in Cdc27 is responsible for directing Cyclin D1 to alternative degradation by the APC/C. Furthermore, they show an overall decrease in Cdc27 expression in breast cancer cell lines (Pawar et al., 2010). The results reported in this dissertation do not align precisely with those reported by Pawar et al., however that may be a result of their focus on the transcriptional regulation of *Cdc27* in response to the transcription factor CEBPδ rather than focusing on translational regulation. Importantly, the finding that increased Cdc27 expression can lead to redirection of SCF substrates to the APC/C is consistent.

Aberrant APC/C activity in cancer Proper APC/C activity has previously been shown to be necessary for the maintenance of genomic integrity (Garcia-Higuera et al., 2008; Penas et al., 2011). Temporal regulation of protein ubiquitination and subsequent degradation allows the forward-only progression through the cell cycle, prevents re-duplication of DNA, and ensures that duplicated chromosomes are divided perfectly equally between daughter cells prior to cytokinesis (Penas et al., 2011; Peters, 2006). Due to its extensive role in regulating cell cycle progression, it is obvious that maintaining proper APC/C activity through regulation of its activating cofactors is essential to

maintaining chromosomal stability. Premature activation of the APC/C during mitosis results in mitotic aberrations such as lagging chromosomes and anaphase bridges, both of which can result in aneuploid chromosome numbers (Listovsky & Sale, 2013). Premature activation of the APC/C^{Cdc20} during G1 leads to premature S phase entry and degradation of APC/C target, geminin, which can result in DNA re-replication (Clijsters, Ogink, & Wolthuis, 2013).

Others have reported on contribution of phosphorylation to the affinity of APC/C core components and cofactors. Several APC/C core subunits are phosphorylated during mitosis, and this phosphorylation was shown to increase ubiquitin ligase activity of the complex (Kramer et al., 2000). Phosphorylation of the cofactor, Cdc20, was also shown to enhance its binding to the core complex; in contrast, the phosphorylation of Cdh1 ablated its ability to bind to the APC/C (Kramer et al., 2000). Atypical kinase activity is often seen in cancer, and might contribute to the overall ability of the APC/C to ubiquitinate targets appropriately. We do not investigate the phosphorylation of the APC/C components here, but recognize the regulatory role that phosphorylation plays in combination with translational regulation of Cdc27.

Cdh1 deletion results in genomic instability and tumorigenesis Cdh1 has been described previously as a tumor suppressor, and is implicated in both centrosome amplification and missegregation of chromosomes (Garcia-Higuera et al., 2008). Levels of Cdh1 are normally regulated during the cell cycle by ubiquitination by the Skp1/Cullin/F-box (SCF) E3 ubiquitin ligase (Benmaamar & Pagano, 2005; Fukushima et al., 2013). The SCF is constitutively active, its specificity dictated by the presence of different cofactors and the recognition of phosphorylated residues, or phosphodegrons, of its substrates

(Fukushima et al., 2013). Thus, the careful regulation of Cdh1 phosphorylation is necessary to guarantee that it is not ubiquitinated and degraded in an untimely fashion. The cofactor responsible for Cdh1 recognition by the SCF is beta-transducin repeating-containing protein (β-TRCP) which recognizes phosphodegrons on Cdh1 after it has been phosphorylated by cyclin-dependent kinase 1 (CDK1) and polo-like kinase 1 (Plk1) (Fukushima et al., 2013). As previously mentioned, proliferative signaling in the absence of growth stimuli commonly occurs during tumor progression (Hanahan & Weinberg, 2000, 2011), and this sustained proliferative signaling can lead to activation of downstream signaling pathways. We consider the role of constitutive activation of the kinases responsible for Cdh1 phosphorylation and recognition by the SCF in this study, as well as the degradation of other SCF substrates. We also consider alternative degradation of Cdh1 by the APC/C, much like the reported APC/C-dependent degradation of Cyclin D1 (Pawar et al., 2010). Loss of Cdh1-mediated APC/C activity results in errors in DNA replication and ultimately contributes to aneuploidy (Engelbert, Schnerch, Baumgarten, & Wasch, 2008).

Chromosomal instability Chromosomal instability is the term used to describe an increased rate in missegregation of chromosomes during cell division, often resulting in net gains or losses in total chromosome number, or aneuploidy. Approximately 90% of carcinomas exhibit aneuploid chromosome numbers (Weaver & Cleveland, 2006). Susceptibility to chromosomal instability is a valuable adaptation acquired by cancer cells in that they exhibit accelerated rates of evolution, conferring increased adaptability to new and changing microenvironments (Heng et al., 2013). Additionally, errors in cell cycle checkpoints often accompany chromosomal instability, allowing cells with DNA damage or aneuploidy to avoid cell cycle arrest and continue proliferating (Bharadwaj & Yu, 2004).

The mechanisms underlying chromosomal instability remain poorly understood. That is, while some causes of chromosomal instability have been identified, such as errors in spindle assembly checkpoint, centrosome duplication, and bipolar spindle attachment (Bakhoum & Compton, 2012; Heng et al., 2013; Nowak et al., 2002), the mechanisms underlying their regulation have not been elucidated. The role of the APC/C in regulating proper chromosomal segregation and initiation of DNA replication underpins its importance in maintaining the genomic integrity of cells. We evaluate the variable expression of APC/C core component, Cdc27, in both breast cancer cell lines and breast cancer patient samples in an attempt to correlate it with chromosomal instability and metastatic recurrence.

***In vivo* selection of cells that metastasize to lung** In the past, others have described a method for *in vivo* selection of cells that metastasize to specific organs by passaging them in mice (Bos et al., 2009; Minn et al., 2005). The purpose of developing such a model is to assess the genetic changes that cells undergo as they progress from the primary tumor site to distant metastases. Organ-specific gene signatures were assigned, with the intent of identifying novel disease biomarkers (Bos et al., 2009; Minn et al., 2005). This and other studies utilizing *in vivo* selection techniques have relied upon cancer cell lines that have already transitioned from normal to malignant cells. With this method in mind, our laboratory has developed a mouse model of metastasis utilizing the non-transformed mouse mammary gland epithelial (NMuMG) cell line. We have shown that knockdown of the RNA binding protein hnRNP E1, a known regulator of the epithelial-to-mesenchymal transition, results in the ability of hnRNP E1 knockdown cells (E1KD) to form tumors and distant metastases *in vivo* when injected into the mammary fat pads of SCID

mice (Chaudhury, Hussey, et al., 2010; Hussey et al., 2011). *In vivo* passaging, which allows for the artificial selection of cells capable of forming primary tumors and lung metastases, can enhance the metastatic potential of the E1KD cell line. This technique led to the isolation of two increasingly aggressive metastatic cell lines, termed L1P, and L2P, that metastasize to lung. In addition, the M1P cell line was isolated from a primary mammary tumor. We believe that we have a unique model system for interrogating changes associated with tumor initiation and metastatic progression: while previous models have utilized cancer cell lines to initiate primary tumors, our model originates from normal, non-metastatic cell line.

III. Chapter 3: Methods

Reagents Primary antibodies: Mouse α-Fzr1, α-Cdc27, α-Securin, and α-Pak1 antibodies were obtained from Abcam. Mouse α-PCBP1 was obtained from Abnova. Rabbit α-APC3, α-phospho-Pak1 (Thr423), α-Cdc20, HRP-conjugated α-phospho-RXXS*/T*, and Alexa fluor 488-conjugated α-alpha tubulin were obtained from Cell Signaling Technology. Mouse α-Hsp90, α-GAPDH, α-Cyclin A, goat α-L1CAM, and α-HnRNP E1 were obtained from Santa Cruz Biotechnology.

Secondary antibodies: HRP-linked sheep α-mouse and donkey α-rabbit were obtained from GE Healthcare Life Sciences, and HRP-linked rabbit α-goat was obtained from Thermo Scientific.

Cell culture and treatments Cells were maintained in tissue culture incubators at 37°C, 5% CO_2, and 95% humidity. Normal murine mammary gland epithelial (NMuMG) cells obtained from American Type Culture Collection (ATCC; Manassas, VA, USA) were maintained in Dulbecco's modified Eagle's medium supplemented with 10% fetal bovine serum (Atlanta Biologicals; Atlanta, GA, USA), 10 μg/ml insulin (Lonza; Allendale, NJ, USA), and antibiotics/antimycotics (100 units/ml penicillin G, 100 mg/ml streptomycin, and 0.25 mg/ml amphotericin B) (Gibco/ThermoFisher; Grand Island, NY, USA). Puromycin was purchased from Sigma-Aldrich (St. Louis, MO, USA) and neomycin (G418) was obtained from Invivogen (San Diego, CA, USA). Stable hnRNP E1-knockdown (E1KD) cells were generated in the laboratory by transfecting NMuMG cells with pSilencer 2.1-U6 (Ambion/ThermoFisher; Grand Island, NY, USA) plasmid containing shRNA targeting hnRNP E1 and a puromycin resistance selection marker. E1KD cells were maintained in the same media as NMuMGs supplemented with 10 μg/ml puromycin. NMuMG-Cdc27 cells

were generated in the laboratory by transfecting NMuMG cells with pECE-M2 plasmid containing the Cdc27 open reading frame. NMuMG-Cdc27 cells were maintained in the same media as NMuMGs supplemented with 10 mg/ml neomycin. E1KD-shCdc27 cells were generated in the laboratory by transducing E1KD cells with pLKO.1 lentiviral particles containing shRNA targeting Cdc27 and a neomycin selection marker. E1KD-shCdc27 cells were maintained in the same media as NMuMGs supplemented with 10 μg/ml puromycin and 10 mg/ml neomycin. The Pak1 inhibitor IPA-3 was purchased from Selleck Chemicals (Houston, TX, USA) used at a concentration of 30 μM for times indicated in figures unless otherwise noted in figures. The proteasome inhibitor MG132 was obtained from Sigma-Aldrich (St. Louis, MO, USA) and was used at a concentration of 10 μM for times indicated in figures.

Plasmids pGEX-6P-Cdh1wt (570) was a gift from Jonathon Pines (Addgene plasmid # 39877). pECE-M2-CDC27 was a gift from Anne Brunet (Addgene plasmid # 31661). pLKO.1 neo was a gift from Sheila Stewart (Addgene plasmid # 13425). pGEX-6P-hnRNP E1wt was a generous gift from Rakesh Kumar.

Cell synchronization Cell synchronization was performed to analyze cell cycle-specific expression of mRNAs and proteins. Cells were synchronized in G0 phase by incubating in DMEM supplemented with 0.5% fetal bovine serum for 16 hours. Synchronization at G0, while convenient, is not highly effective at synchronizing the entire population of cells on a tissue culture plate. Because of this, double-thymidine block was used to effectively synchronize populations of cells at G1/S. Briefly, 2 mM thymidine was added to culture media and cells were incubated for 16 hours. The media was removed after 16 hours and plates were washed with sterile 1X PBS three times, then released for 9

hours by addition of complete medium. Cells were then blocked again by addition of 2 mM thymidine. Cells were synchronized in mitosis by first blocking with 2 mM thymidine for 16 hours, then washing three times in 1X sterile PBS and releasing directly into complete medium supplemented with 50 ng/mL nocodazole for 12 hours. Mitotic cells were harvested after 12 hours of incubation with nocodazole, or washed three times in 1X sterile PBS and released into complete medium to allow cells to complete mitosis and progress into early G1 phase. G1 cells were harvested 4 hours after release from nocodazole block.

DAVID analysis of hnRNP E1-regulated genes Affymetrix array analysis was performed previously (Hussey et al., 2012) to generate a dataset containing genes that are post-transcriptionally regulated by hnRNP E1. Enrichment of biological processes and pathways in the geneset was assessed using the DAVID webtool (Huang, Sherman, & Lempicki, 2008, 2009). The cutoff for gene expression change between NMuMG monosome and E1KD polysome samples was 1.5 fold.

Whole cell lysate preparation Whole cell lysates were prepared by aspirating culture medium, then washing cultured cells three times with ice cold 1X phosphate-buffered saline (PBS). RIPA lysis buffer with protease and phosphatase inhibitors was added directly to cells. Cells were scraped and transferred to microfuge tubes, incubated on ice 10 minutes, sonicated, then centrifuged at high speed. Supernatants were transferred to new tubes and protein content was measured by Bradford assay using known dilutions of bovine serum albumin to generate a standard curve. Bradford Protein Assay reagent was obtained from Bio-Rad (Hercules, CA, USA) and absorbance was measured at 595 nm on a Perkin Elmer Wallac 1420 Victor2 microplate reader (Perkin Elmer; Waltham, MA, USA).

Immunoblot analysis To assess protein expression in cells, whole cell lysates prepared as described above were denatured by addition of 4X sample buffer (to 1X dilution) and boiling for 5 minutes at 95°C. Lysates were then resolved by denaturing SDS-polyacrylamide gel electrophoresis (SDS-PAGE) and transferred to polyvinylidene difluoride (PVDF) membrane. Membranes were blocked to prevent nonspecific binding of antibody in 5% milk in 1X TBS-T or 5% bovine serum albumin in 1X TBS-T for 30 minutes at room temperature. Primary antibodies were diluted 1:1000 in 5% milk/TBS-T or 5% BSA/TBS-T and membranes incubated overnight at 4°C with gentle rocking. Membranes were washed three times for 15 minutes each in 1X TBS-T, and then incubated in secondary antibody (diluted 1:10,000 in 5% milk/TBS-T) for 1 hour at room temperature. Membranes were washed three times for 15 minutes each in 1X TBS-T, then Luminata Forte Western HRP substrate (EMD Millipore; Billerica, MA, USA) was added and membranes were exposed using Bio-Rad ChemiDoc MP system (Bio-Rad; Hercules, CA, USA).

Reverse transcription of total RNA To assess expression of mRNAs in cells, total RNA was isolated from cells using Trizol reagent (Life Technologies/ThermoFisher; Grand Island, NY, USA) according to the manufacturer's protocol. Complementary DNA (cDNA) was transcribed from 2 μg total RNA using M-MLV reverse transcriptase (Sigma Aldrich; St. Louis, MO, USA) and oligo dT primers (Invitrogen/ThermoFisher; Grand Island, NY, USA).

Semi-quantitative polymerase chain reaction (PCR) PCR was performed using Maxima Hot-Start Taq DNA polymerase (Life Technologies/ThermoFisher; Grand Island, NY, USA). PCR products were electrophoresed on 2% agarose gels stained with ethidium

bromide and visualized using BioRad ChemiDoc system. Primer sequences are described in Table 1.

Gene	Primer Sequence
Cdc27 forward	5' – TGGGTCAAACTCATCTCGCC – 3'
Cdc27 reverse	5' – GGTGACGAATGACGGCAATG – 3'
Actb forward	5' – TCATGAAGTGTGACGTTGACATCCGT – 3'
Actb reverse	5' – CCTAGAAGCATTTGCGGTGCACGATG – 3'
L1CAM forward	5' – GTCCCTCACGTTGGGAATGT – 3'
L1CAM reverse	5' – AGAGGGCTCATCAACAGACC – 3'
Fzr1 forward	5' – CGTGACCGCATGATCCTACA – 3'
Fzr1 reverse	5' – TGTGTGCTCACCAGCTCATT – 3'
pSilencer forward	5' – CAGTGCTGCAATGATACCGC – 3'
pSilencer reverse	5' – GGGAACCGGAGCTGAATGAA – 3'

Table 1: Gene-specific sequences of primers used for PCR.

S100 Fraction Cell Lysate Preparation S100 fractions were utilized for polysome profile analysis. The S100 fraction of a cell lysate specifically contains the cytoplasmic contents of cells, and since ribosomal translation occurs in the cytosol. S100 fractions were prepared by washing cultured cells three times in ice cold 1X PBS. S100 lysis buffer was added directly to cells and they were scraped and transferred to microfuge tubes. Lysates were passed through 26G needles ten times on ice, then incubated on ice 10 minutes and finally centrifuged at 10,000 x g for 5 minutes. Supernatants were transferred to new tubes and kept on ice for immediate use.

Polysome profile analysis Polysome profile analysis determines the level at which a transcript is being translated into protein, sedimenting mRNA based on its density, which is proportional to the number of ribosomal subunits with which it is associated. Those mRNAs being translated at a high rate will sediment to heavier fractions, as they contain many complete 80S ribosomes, whereas poorly translating mRNAs will sediment to lighter fractions, as they contain fewer ribosomes. S100 fractions were layered onto 10-50% sucrose density gradients and centrifuged at 35,000 x g for 3 hours at 4°C. Fractions were then removed from the column by pushing 80% sucrose from the bottom of the gradient and removing fractions from the top. Absorbance at 254 nanometers was recorded for each fraction as it was collected.

Immunoprecipitations There is currently no primary antibody to detect phospho-hnRNP E1 directly, so an indirect approach was utilized where hnRNP E1 was immunoprecipitated from whole cell lysates, then assayed by immunoblot for phosphoserine or phosphothreonine. Immunoprecipitations were carried out by incubating 1 mg whole cell lysate with 5 μg Abnova α-PCBP1 primary antibody in a volume of 500 μl overnight at 4°C with end-over-end rotation. Protein A-sepharose beads were washed three times in RIPA lysis buffer, and then 50 μl beads were added to each sample and incubated at 4°C with end-over-end rotation for a minimum of 3 hours. After incubation, beads were washed a minimum of five times with RIPA lysis buffer, then transferred to a new tube before removing all wash buffer from the beads and adding 50 μl 1X Laemmli sample buffer. Samples were boiled for 5 minutes before being loaded onto SDS-PAGE gels, electrophoresed, and transferred to PVDF membrane for subsequent immunoblot analysis.

RNA-immunoprecipitation To assay mRNA binding to hnRNP E1 protein, hnRNP E1 was immunoprecipitated from lysates followed by RNA isolation. RNA-immunoprecipitations were performed as described above with some minor modifications. Briefly, all buffers were prepared in diethyl pyrocarbonate-treated water and RNase inhibitors were added to the antibody-lysate mixture for overnight incubation. After final washing of beads and transfer to new microfuge tubes, all wash buffer was removed and Trizol reagent was added to isolate RNA bound to the immunoprecipitated hnRNP E1. Total RNA was prepared according to Trizol manufacturer's instructions. Total RNA was reverse-transcribed into cDNA as described above, and semi-quantitative PCR was performed as described above.

Site-directed mutagenesis Site-directed mutagenesis was performed to mutate pGEX-6P-hnRNP E1wt plasmid using Agilent QuikChange Site-Directed Mutagenesis Kit (Agilent Technologies; Santa Clara, CA, USA) according to the manufacturer's protocol. Primers were designed using QuikChange Primer Design Program (Agilent Technologies; Santa Clara, CA, USA). Single mutations were carried out sequentially and DNA sequencing was performed by Genewiz (Genewiz; South Plainfield, NJ, USA) on plasmids to validate mutation.

***In vitro* kinase assay** Pak1 kinase was immunopurified from synchronized NMuMG cell lysates prepared in kinase lysis buffer. To isolate the kinase, 250 μg of lysate was incubated with 2.5 μg α-Pak1 antibody (Abcam; ab40852) and 30 μl Protein A Sepharose (GE Life Sciences) beads in a total volume of 250 μl for 4 hours at 4°C with end-over-end rotation. Complexes were collected by centrifugation at 2,000 rpm for 3 minutes and washed five times in ice-cold kinase lysis buffer. After washing, the supernatant was totally

removed from kinase/bead complexes and they were immediately resuspended in 30 μl kinase assay buffer. Kinase reactions were initiated by adding 5 μg substrate protein [GST-WT-hnRNP E1, GST-phosphomutant-hnRNP E1, or recombinant Histone H4 (New England Biolabs)] and 0.5 μCi [γ^{32}P]-ATP (Perkin Elmer; 3000 Ci/mmol) in 20 μl kinase buffer. The reaction was allowed to proceed at 30°C for 20 minutes, then terminated with the addition of 1X Laemlli sample buffer and heating to 95°C for 2 minutes. Samples were resolved by SDS-PAGE on a 15% reducing polyacrylamide gel and analyzed by autoradiography.

***In vitro* ubiquitination assay** APC/C was affinity purified from synchronized whole cell lysates to compare E3 ligase activity at different phases of the cell cycle in different cell lines. Protein A-Sepharose beads (GE Healthcare Life Sciences; Marlborough, MA, USA) and α-Cdc16 (sc365636 - Santa Cruz Biotechnology; Dallas, TX, USA) antibody were conjugated by overnight incubation with end-over-end rotation at 4°C. Cells were synchronized as described above, using thymidine-nocodazole block and release to isolate mitotic-APC/C and G1-APC/C, respectively. Plates were washed three times in 1X ice-cold PBS, then scraped and centrifuged in PBS to obtain cell pellets. Pellets were lysed in 3 pellet volumes of ubiquitination lysis buffer. Lysates were incubated with 10 μl antibody/beads at 4°C for 2 hours in a volume of 100 μl. Affinity-purified APC/C was washed on beads three times in 1X TBS-T. To initiate ubiquitination reactions, immunoprecipitates were incubated with 200 nM recombinant substrate (myc-Cyclin B1 residues 1-102 or full-length GST-Cdh1), 1X ubiquitination reaction buffer, 250 nM UBE1 (ubiquitin activating enzyme) (Boston Biochem; Cambridge, MA, USA), 1 μM His-UbcH10 (ubiquitin conjugating enzyme), 1 μM His-Ube2S (ubiquitin conjugating enzyme), 1 mg/ml creatine phosphokinase (Sigma-Aldrich; St. Louis, MO, USA), to a volume of 10 ul with water. Reactions were incubated at

37°C for 1 hour with shaking at 1000 rotations per minute. To stop reactions, 5 μl Laemmli sample buffer was added and reactions were vortexed. Reactions were loaded onto 10% SDS-polyacrylamide gels for electrophoresis and subsequent immunoblot analysis. Myc-Cyclin B1, His-UbcH10, and His-Ube2S were generous gifts of Dr. Aaron Tipton (Oklahoma Medical Research Foundation; Oklahoma City, OK, USA).

Flow cytometry To evaluate the distribution of populations of cells throughout the cell cycle, propidium iodide staining of DNA and subsequent flow cytometric analysis was performed. Cultured cells were trypsinized and centrifuged at 1000 rpm for 3 minutes to pellet. After decanting culture media, pellets were resuspended in 300 μl 1X PBS and 700 μl of 100% ethanol was added drop-wise with low-speed vortexing. Cells were incubated at 4°C overnight to fix and permeabilized completely. To ensure that only cellular DNA was stained, RNase A was added at a concentration of 8 μg/ml and the suspensions were incubated at 4°C for an hour to allow complete degradation of cellular RNA. Propidium iodide was then added to samples at a concentration of 50 μg/ml and samples were transferred to flow cytometry tubes after being strained through 40 μm cell strainers. Samples were incubated in the dark for at least 30 minutes at 25°C, and then analyzed using a BD FACSAria (BD Biosciences; San Jose, CA, USA) flow cytometer and FACSDiva (BD Biosciences; San Jose, CA, USA) software. Data was then analyzed using FCS Express 5 Plus software (De Novo Software; Glendale, CA, USA). Cells were gated first by plotting forward scatter height versus side scatter height to separate cells from cellular debris. The gated population was then gated again by plotting propidium iodide width versus propidium iodide area. This allowed for the gating of single cells. Histograms were then prepared from the gated single cell populations and distribution of cells in cell cycle phases was analyzed

using the MultiCycle AV DNA Analysis Plug-in of FCS Express 5 Plus software, specifically utilizing the Dean-Jett mathematical model of DNA distribution (Dean & Jett, 1974).

Immunocytochemistry Immunocytochemistry was performed using fluorescence-labeled primary antibodies and DAPI. Cells were cultured on glass coverslips in 6 well tissue culture plates. To prepare coverslips for mounting onto slides, culture media was aspirated and cells were fixed by incubating in 4% paraformaldehyde prepared in 1X PBS for 20 minutes at 25°C with gentle rocking. Cells were washed three times for 10 minutes each in 1X PBS, then permeabilized and blocked simultaneously by incubating 2% BSA and 0.2% Triton X-100 prepared in 1X PBS (blocking buffer) for 1 hour at 25°C with gentle rocking. Alexa fluor 488-conjugated α-alpha Tubulin antibody was diluted 1:1000 in blocking buffer and added to wells to cover coverslips, then incubated in the dark for 1 hour at 25°C with gentle rocking. Cells were washed again three times in 1X PBS for 10 minutes each. A single drop of mounting medium with DAPI was added to a microscope slide, and then coverslips were carefully removed from wells of plate using fine forceps and placed on slides, cells down. Coverslips were sealed using clear nail polish and allowed to dry in the dark before imaging slides using an Olympus FV10i laser scanning confocal microscope.

Metaphase spread analysis To determine the percentage of aneuploid metaphase chromosomes in a cell line, metaphase chromosome spreads were prepared. Cells were cultured in colcemid (KaryoMAX/ThermoFisher; Grand Island, NY, USA) at a final concentration of 1 μg/ml at 37°C for 1 hour. Culture media was aspirated and cells washed in 1X PBS, then trypsinized and centrifuged at 1000 rpm for 4 minutes to pellet. The supernatant was decanted and the pellet was resuspended in the remaining media

(approximately 200 μl) by gentle trituration. 5 ml of ice-cold 0.56% potassium chloride was added to swell the cells and incubated at 25°C for 6 minutes, then cells were centrifuged at 1000 rpm for 4 minutes to pellet again. After decanting supernatant, pellets were resuspended in the remaining volume of potassium chloride solution by gentle trituration. Ice-cold fixative (3:1 methanol: glacial acetic acid) was added drop-wise to cells while vortexing on low speed. The suspension was centrifuged at 1000 rpm for 4 minutes to pellet fixed cells. The fixative was decanted and cell pellets were resuspended in 1 ml fixative. A small volume (20 μl) of fixed cell suspension was released in single drops from a height of approximately 50 cm onto clean, dry microscope slides over a beaker of warm water. At least 2 slides were prepared per cell line. Slides were allowed to dry overnight, and then mounting medium with DAPI was added to slides and coverslips placed and sealed with clear nail polish. Metaphases were imaged using an Olympus FV10i laser scanning confocal microscope and counted using ImageJ software (National Institutes for Health; Bethesda, MD, USA) with the cell count plugin. At least 50 metaphases were counted per cell line.

Generation of *in vivo* selected M1P, L1P, and L2P cell lines Nonobese diabetic severe combined immunodeficient (NOD/SCID) mice were supplied by the National Cancer Institute (NCI; Bethesda, MD, USA). The Institutional Animal Care and Use Committee at Medical University of South Carolina approved all mouse procedures performed. To generate cells that were increasingly aggressive in breast-to-lung metastasis, 50,000 E1KD cells suspended in 100 μl sterile 1X PBS were injected subcutaneously into the inguinal mammary gland fat pads of 6 week-old NOD/SCID females using 1 CC syringe and 26G hypodermic needle. After 15 weeks, mice were euthanized using CO_2 inhalation and

cervical dislocation. Primary tumors and lungs were excised in sterile conditions, and then tissue was enzymatically dissociated as follows: tumors or lungs were incubated with DMEM and 300 U/ml collagenase and 100 U/ml hyaluronidase (StemCell Technologies; Vancouver, British Columbia, Canada) at 37°C for 4 hours with gentle agitation at 100 rpm. Following enzymatic dissociation, cells centrifuged at 350 x *g* for 5 minutes, supernatant decanted, then resuspended in a 1:4 mixture of cold Hank's Balanced Salt Solution (HBSS) (StemCell Technologies) supplemented with 2% FBS and ammonium chloride (StemCell Technologies). Cells were centrifuged at 350 x *g*, supernatant decanted, then resuspended in 5 ml pre-warmed Trypsin-EDTA, then gently triturated for 1 minute to lyse dead cells. 10 ml of HBSS/2% FBS were added, then cells were centrifuged for 5 minutes at 350 x *g*. Supernatant was decanted and 2 ml of pre-warmed 5 mg/ml Dispase (StemCell Technologies) and 200 μl 1mg/ml DNase I (StemCell Technologies) were added to cell pellets and gently triturated for 1 minute to digest cellular DNA released by dead cells. 10 ml HBSS/2% FBS were added to suspensions, and they were centrifuged again at 350 x *g* for 5 minutes. Resulting cell pellets were resuspended in complete DMEM plus 1 mg/ml puromycin, and then passed through 40 μm cell strainers to generate single cell suspensions. Cells were plated on 10 cm culture dishes and maintained in DMEM with 1 mg/ml puromycin. To generate more aggressive E1KD cells, 50,000 L1P cells were injected into the inguinal mammary fat pads of NOD/SCID females as described previously, and resulting lung metastases were isolated as described above after 5 weeks due to significant morbidity.

***In vitro* migration** Migration was assessed using the CytoSelect™ 24-Well Wound Healing Assay (Cell Biolabs). Briefly, wound-healing inserts were removed from confluent monolayers and cells were fixed and stained 24 hours after removal of inserts.

3D *in vitro* invasion Invasion of E1KD progression series cells was assessed using the Trevigen spheroid invasion assay as per manufacturer's instructions. Briefly, a volume of 50ml single cell suspension in spheroid formation ECM was prepared at a density of 3000 cells per well of a round-bottomed low-attachment 96 well plate. Once seeded, plates were centrifuged at 200 g for 3 min, followed by incubation at 37°C/ 5% CO_2 for 48 hours. A volume of 50ml invasion matrix was added per well of plates placed on ice for 15 min to cool. Following addition of matrix, plates were centrifuged at 300 g for 3 min and incubated for 1h at 37°C to allow matrix to solidify prior to addition of 100ml chemoattractant (DMEM supplemented with 10%FBS and 20ng/ml EGF). Invasive protrusions from spheroids were imaged between 5 and 7 days of matrix addition.

***In vivo* lung colonization assay** 100,000 E1KD, L1P, or L2P cells were injected via tail vein into 6 week-old NOD/SCID female mice. Cells were suspended in 100 μl sterile 1X PBS and injections were performed using a 28G sterile hypodermic needle and 1 CC syringe. Mice were euthanized after 6 weeks using CO_2 inhalation and cervical dislocation. Lungs were formalin-fixed and paraffin embedded for immunohistochemical analysis.

Immunohistochemistry Formalin-fixed paraffin-embedded lungs from mice that had undergone tail vein injections of E1KD, L1P, and L2P cells were processed by the Medical University of South Carolina Center for Oral Health Research (MUSC COHR). Briefly, 5 μm sections were cut using a microtome, deparaffinized, and then stained using hematoxylin and eosin. Histopathological analysis was performed by the MUSC COHR.

Tissue Microarray and Immunohistochemistry Tissue microarray (TMA) compilation and immunohistochemical staining was performed by the Hollings Cancer Center Biorepository and Tissue Analysis core. The TMAs contained matched normal and tumor tissue samples, as well as normal and metastatic lymph node tissue from patients for whom survival data was made available (Table 3). For immunohistochemical staining of formalin-fixed, paraffin-embedded TMAs and mouse lung tissue, sections were deparaffinized in xylene, rehydrated in ethanol and processed as follows: the sections were incubated with target retrieval solution (S2367; Dako, Carpinteria, CA, USA) in a steamer for 45 min followed by 3% hydrogen peroxide solution for 10 min and protein block (X0909; Dako) for 20 min at room temperature. Sections were incubated overnight in a humid chamber at 4^{o}C with α-Cdc27 (Abcam; dilution of 1:1000, pH 9.0) or α-Fzr1 (Abcam; dilution of 1:2000, pH 6.0) antibodies followed by biotinylated secondary antibody (PK6106; Vector laboratories, Burlingame, CA, USA) for 30 min and ABC reagent for 30 min. Immunocomplexes of horseradish peroxidase were visualized by DAB reaction (K3468; Dako), and sections were counterstained with hematoxylin before mounting. Micrographs of stained sections were taken using an Olympus DP72 8-bit RGB camera with Cellsens acquisition software. Images were stitched together using Microsoft ICE.

Statistical analysis of tissue microarray results Staining of tissue microarray samples was scored on a scale of 0 to 3 by three separate individuals. Scores were averaged and statistical analysis was performed by two-tailed Student's *t*-test of pair-wise comparisons or one-way ANOVA followed by Tukey's *post hoc* test. Kaplan-Meier survival curves were analyzed using MedCalc Statistical Software (MedCalc Software; Ostend,

Belgium) with significance determined by the Logrank test. $P<0.05$ were considered statistically significant.

IV. Chapter 4: Results

HnRNP E1 regulates translation of mRNAs involved in several cellular processes. Previously, we showed that hnRNP E1 represses translation of specific mRNAs involved in epithelial-to-mesenchymal transition (EMT) by binding to their 3' UTRs in a TGFβ-sensitive manner (Chaudhury, Hussey, et al., 2010; Hussey et al., 2011). We established a TGFβ-induced hnRNP E1-dependent EMT gene signature by combining polysome profiling with Affymetrix array analysis in normal mouse mammary epithelial (NMuMG) cells and NMuMGs in which hnRNP E1 had been stably silenced (E1KD) (Hussey et al., 2012). To better understand the role of hnRNP E1 outside of TGFβ-mediated translational regulation and EMT, the array data collected was filtered to identify those mRNAs whose expression was 1.5-fold higher in the monosome fractions of NMuMGs and 1.5-fold higher in the polysome fractions of E1KDs, independent of TGFβ. The mRNAs were then subject to pathway analysis using DAVID functional annotation software. Many biological pathways were significantly enriched in this dataset, including cell cycle (Fig. 1A). Of the genes identified as both hnRNP E1-dependent and involved in cell cycle (Fig. 1B), Cdc27 was of particular interest because of its role as a core component of the anaphase promoting complex/cyclosome, an E3 ubiquitin ligase that plays an integral role in maintaining chromosomal integrity.

In order to validate the results of the array, total RNA and protein expression levels were assessed in NMuMG and E1KD cells. While levels of *Cdc27* transcript remained unchanged between cell lines, the level of Cdc27 protein was higher in E1KD cells (Fig. 2A, upper). Polysome profile analysis was performed to validate translational regulation and

Cdc27 mRNA primarily sedimented to the light monosomal fractions in NMuMGs in contrast to its sedimentation to the dense polysomal fractions in E1KDs (Fig. 2B, lower).

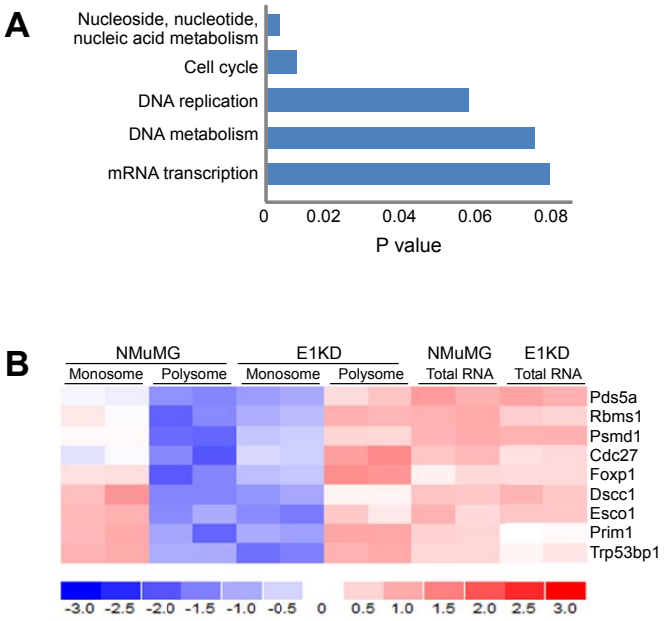

Figure 1: HnRNP E1 regulates translation of mRNAs in many biological processes. (A) DAVID functional annotation analysis of translationally-regulated genes identified in Affymetrix array of monosomal NMuMG genes and polysomal E1KD genes (Student's *t*-test, fold change > 1.5 between groups and < 1.5 within groups). Genes were annotated using Panther biological processes. (B) Heat map showing differential signal strength intensities for cell cycle genes between NMuMG and E1KD monosomes and polysomes compared to total, unfractionated mRNA.

HnRNP E1 regulates Cdc27 expression at the translational level in a cell cycle-dependent manner. Since Cdc27 is involved in cell cycle regulation, we hypothesized that its expression might fluctuate with regard to cell cycle phase. To assess this, NMuMG and E1KD cells were synchronized at G0 by culturing in DMEM with 0.5% FBS for 16 hours. Cells were then stimulated using 10% fetal bovine serum and whole cell lysates and total RNA were collected at the indicated time points. In the NMuMG cells, Cdc27 expression is

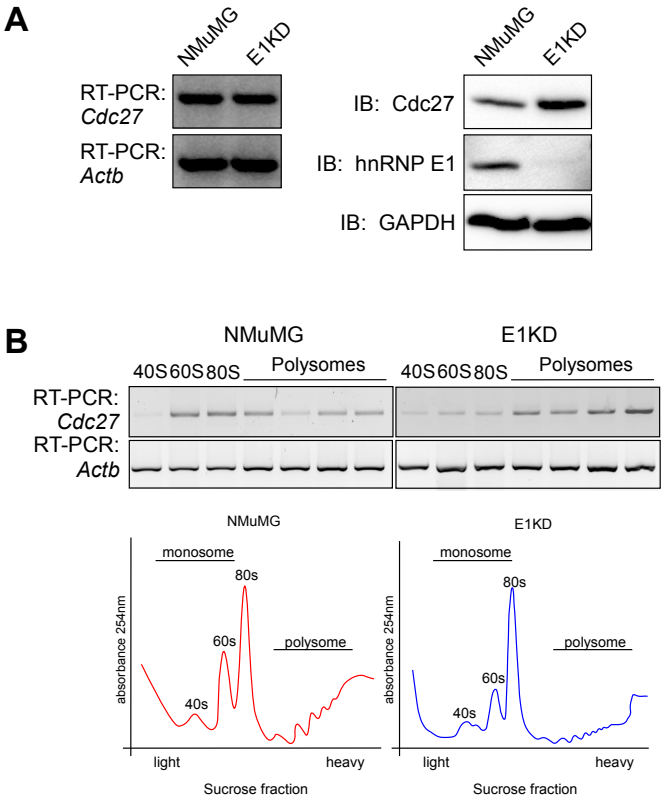

Figure 2: Cdc27 expression is upregulated translationally in E1KD cells compared to NMuMG cells. (A) *Left* Semi-quantitative RT-PCR using gene specific primers to *Cdc27* and *Actb* (control) on total RNA isolated from asynchronous populations of NMuMG and E1KD cells. *Right* Immunoblot analysis examining protein expression levels of Cdc27, hnRNP E1, and GAPDH (control) in whole cell lysates isolated from asynchronous NMuMG and E1KD cells. (B) *Upper* Semi-quantitative RT-PCR using gene specific primers to *Cdc27* and *Actb* (control) on polysome profiles of asynchronous NMuMG and E1KD cells. *Lower* Traces of A254 profiles resulting from NMuMG and E1KD polysome profiling.

increased at the protein level during progression through the cell cycle (Fig. 3A) while no change is observed in total mRNA (Fig. 3B). Progression through the cell cycle was validated by propidium iodide staining of total cellular DNA followed by flow cytometric analysis (Fig. 4). In the E1KD cells, Cdc27 expression is constitutively high throughout the

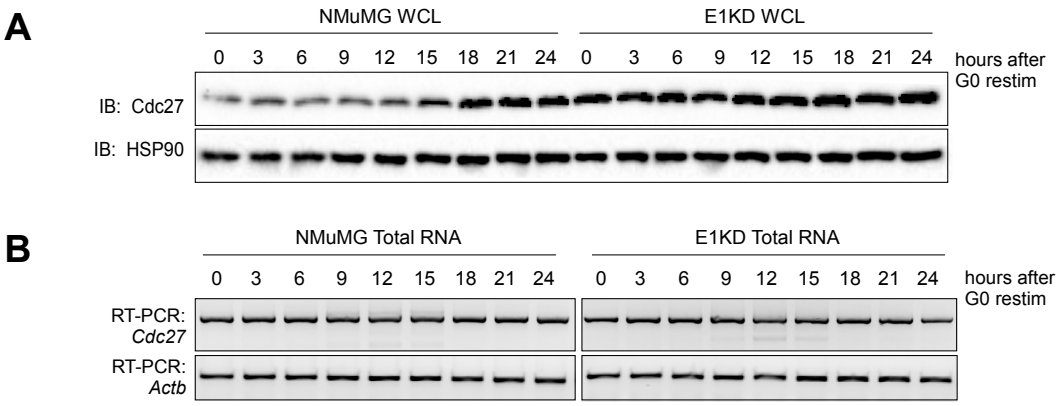

Figure 3: Cdc27 expression is regulated at the protein level and not the mRNA level during the cell cycle. (A) Immunoblot analysis of protein expression of Cdc27 and Hsp90 (control) in NMuMG and E1KD cells that were synchronized by overnight culturing in DMEM + 0.5% FBS then released by addition of complete medium. (B) Semi-quantitative RT-PCR using gene specific primers for *Cdc27* and *Actb* (control) on total RNA isolated from NMuMG and E1KD cells that were synchronized as in (A) above.

cell cycle (Fig. 3A) with no observable change in total mRNA transcript levels (Fig. 3B). Polysome profile analysis was repeated to validate the microarray findings. Cytosolic extracts from synchronized NMuMGs and E1KDs were subject to polysome profile analysis: *Cdc27* mRNA sediments to monosomal fractions in G0-synchronized NMuMGs and to polysomal fractions after 24 hour restimulation with complete medium; *Cdc27* mRNA sediments to the polysomal fractions irrespective of cell cycle phase in E1KDs (Fig. 5A).

To determine whether *Cdc27* mRNA and hnRNP E1 interact directly within the cell, RNA-immunoprecipitation was performed. Immunoprecipitation of hnRNP E1 from synchronized cytosolic cell extracts followed by RNA isolation and semi-quantitative RT-PCR reveals that *Cdc27* mRNA binds hnRNP E1, and this binding is lost upon mitogenic stimulation (Fig. 5B). *L1CAM* mRNA binding to hnRNP E1 has been included as a positive

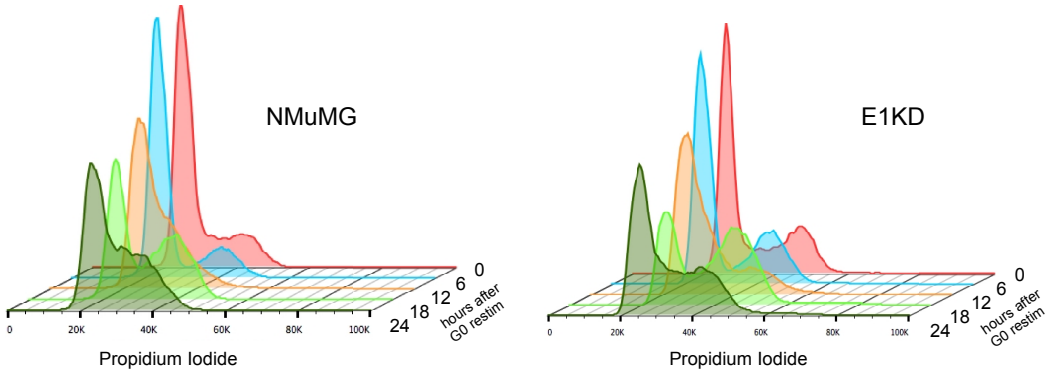

Figure 4: Progression of G0-synchronized NMuMG and E1KD cells through the cell cycle. Histograms representing propidium iodide staining in G0-synchronized populations of NMuMG and E1KD cells. Cells were synchronized by culturing in DMEM + 0.5% FBS overnight, then releasing into complete medium. Cells were gated from debris, then gated again on singlets to obtain analyses of populations of single cells.

control, as it has been shown by others that hnRNP E1 protein and *L1CAM* mRNA interact in a cell cycle-dependent manner. *Actb* mRNA is included as a negative control, as well as immunoprecipitation carried out using IgG instead of antibody. Input samples are included to show equal loading of protein in immunoprecipitation reactions.

Pak1 phosphorylates HnRNP E1 in a cell cycle-dependent manner, allowing for Cdc27 translation. Because Cdc27 expression did not increase with TGFβ stimulation, other potential kinases were considered for cell cycle-dependent hnRNP E1 phosphorylation. It has been shown previously by others that p21-activated kinase 1 (Pak1) phosphorylates hnRNP E1 in response to mitogenic stimulation (Meng et al., 2007). To assess whether Pak1 might phosphorylate hnRNP E1 during the cell cycle, immunoprecipitation was performed on NMuMG cell extracts that had been synchronized by double thymidine block, then released with or without the Pak1-specific inhibitor, IPA-3.

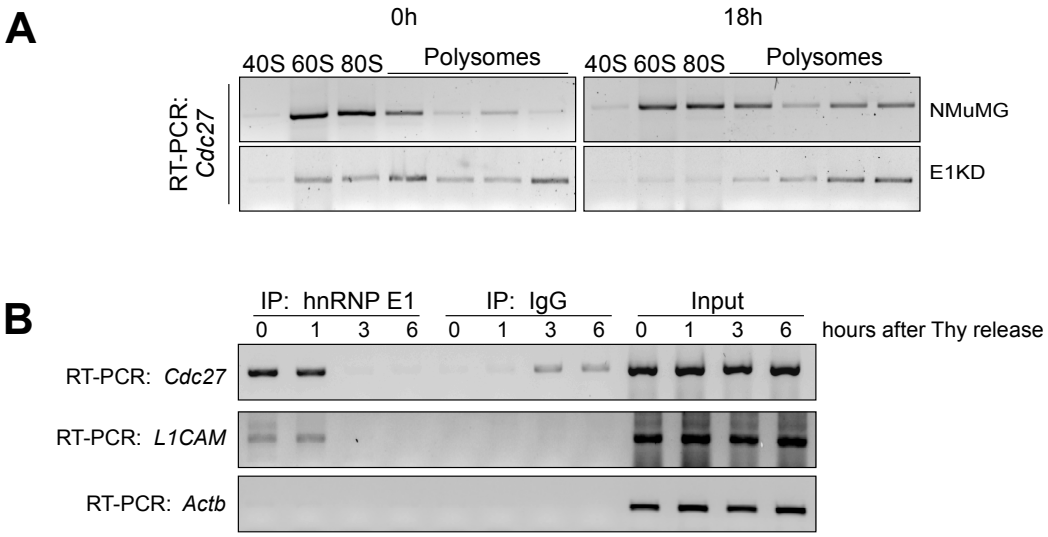

Figure 5: Cdc27 expression is regulated translationally during the cell cycle and interacts directly with hnRNP E1 in a cell cycle-dependent manner. (A) Semi-quantitative RT-PCR analysis using gene specific primers for *Cdc27* using RNA isolated from NMuMG and E1KD polysome profiling of G0-synchronized and cells released for 18 hours. (B) Semi-quantitative RT-PCR using gene specific primers for *Cdc27, L1CAM,* and *Actb* (control) using RNA isolated from anti-hnRNP E1 immunoprecipitates. HnRNP E1 was immunopurified from NMuMG cell extracts synchronized at G1/S by double-thymidine block, then released for times indicated in the figure.

α-hnRNP E1 antibody or IgG were used with Protein A Sepharose beads to immunopurify hnRNP E1 from the cell extracts, then immunopurified hnRNP E1 was resolved by SDS-PAGE. Immunoblot analysis was performed using antibody that recognizes substrates of arginine-directed kinases. The motif recognized is RXXS*/T*, where the serine or threonine with the asterisk is phosphorylated. The two Pak1 phosphorylation sites on hnRNP E1 identified by Meng et al. (threonine 60 and threonine 127) both have an arginine at the -3 position. An increase in phosphorylated hnRNP E1 can be observed following release from

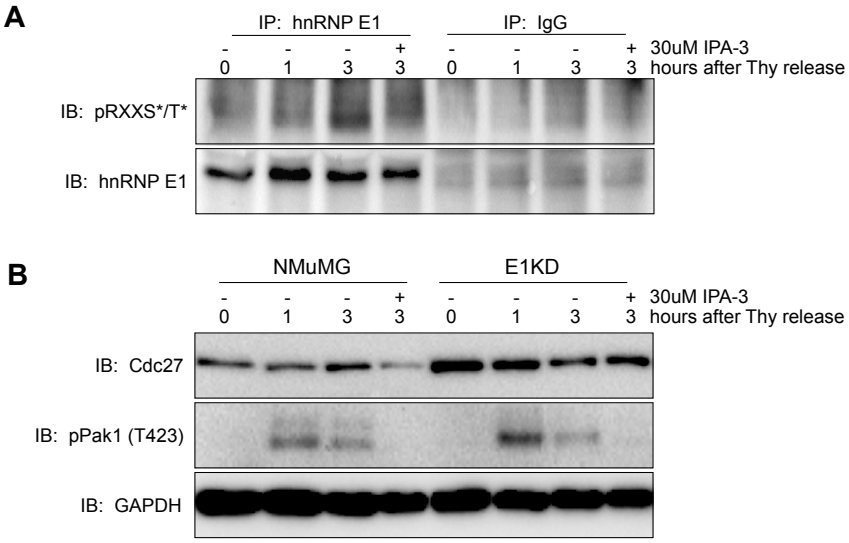

Figure 6: HnRNP E1 is phosphorylated *in vivo* during the cell cycle coinciding with Cdc27 expression. (A) Immunoblot analysis of phosphorylated-RXXS*/T* from anti-hnRNP E1 or IgG (control) immunoprecipitates isolated from NMuMG cells synchronized at G1/S using double-thymidine block, then released -/+ the Pak1-specific inhibitor, IPA-3 for times indicated in the figure. Membrane was stripped and re-probed using anti-hnRNP E1 antibody. (B) Immunoblot analysis of protein expression using anti-Cdc27, anti-phospho-Pak1, and anti-GAPDH (control) whole cell lysates isolated from NMuMG and E1KD cells synchronized and released -/+ IPA-3 as described above.

thymidine block, and this increase in phosphorylation is inhibited by the presence of IPA-3 (Fig. 6A). The membrane was then stripped and re-probed using α-hnRNP E1 antibody to show equal loading.

Pak1, like many kinases, is activated by phosphorylation (Maroto, Ye, von Lohneysen, Schnelzer, & Knaus, 2008). To assess the temporal activation of Pak1 in relation to hnRNP E1 phosphorylation and Cdc27 expression, NMuMG cells were synchronized at the G1/S transition using double thymidine block, then released in the presence or absence

of Pak1 inhibitor, IPA-3. Immunoblot analysis of cell extracts with α-phospho-Pak1 antibody was performed, and phosphorylation of Pak1 kinase can be observed shortly after release from G1/S arrest (Fig. 6B), and this phosphorylation is inhibited in the presence of IPA-3. This phosphorylation event precedes the observed increase in Cdc27 expression (Fig. 6B). Furthermore, inhibition of Pak1 activation by the Pak1-specific inhibitor IPA-3 results in decreased Cdc27 expression in NMuMGs, but not in the E1KDs (Fig. 6B). GAPDH was used as a loading control for the experiment (Fig. 6B).

To determine whether the Pak1 inhibitor, IPA-3, had any effect on hnRNP E1 and *Cdc27* mRNA interaction, RNA-immunoprecipitation was performed in the presence of increasing concentrations of IPA-3. NMuMG cells were arrested using double thymidine block, then released in the presence or absence of 30 μM, 40 μM, or 50 μM IPA-3. Cells were lysed and immunoprecipitation was performed using cell extracts and α-hnRNP E1 antibody or IgG. Release of *Cdc27* mRNA from hnRNP E1 was observed at 3 hours and was inhibited in the presence of Pak1 inhibitor (Fig. 7).

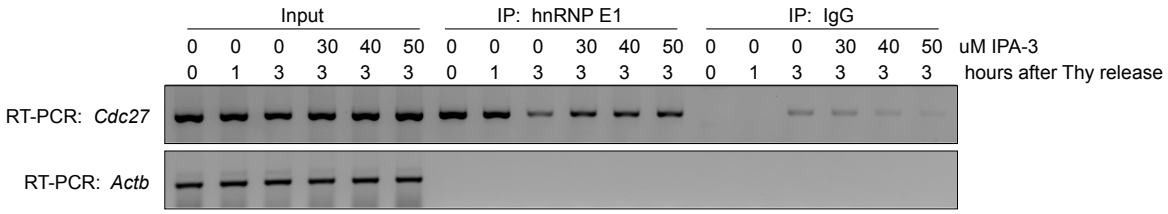

Figure 7: Cdc27 mRNA interacts with hnRNP E1 directly, and this interaction is stabilized by the addition of IPA-3. Semi-quantitative RT-PCR using gene specific primers for *Cdc27* and *Actb* (control) from RNA isolated from hnRNP E1 immunoprecipitates. HnRNP E1 was immunopurified from NMuMG cells synchronized at G1/S using double-thymidine block, the release -/+ increasing concentrations of IPA-3, indicated in the figure.

Finally, we show that endogenous Pak1 can phosphorylate recombinant GST-hnRNP E1 *in vitro.* GST-tagged wild-type hnRNP E1 was used, as well as GST-tagged phospho-mutant hnRNP E1 in which threonine 60 and threonine 127 were both mutated to alanine. Recombinant histone H4 was used as a positive control, as it is a known substrate of Pak1 (Maroto et al., 2008). Whole cell extracts were isolated from NMuMGs that had been synchronized at G1/S by double-thymidine block and then released into S phase by removal of thymidine and mitogen stimulation. Pak1 was affinity-purified from the whole cell extracts using α-Pak1 antibody and Protein A Sepharose beads. The immunopurified kinase was then incubated with GST-WT-hnRNP E1, GST-T60A, T127A-hnRNP E1, or recombinant histone H4 in the presence of [Υ^{32}P]-ATP. *In vitro* phosphorylation of both GST-WT-hnRNP E1 and recombinant histone H4 by immunopurified Pak1 increases after mitogen stimulation (Fig. 8). The phospho-mutant GST-T60A, T127A-hnRNP E1 is not phosphorylated *in vitro* by immunopurified Pak1 (Fig. 8).

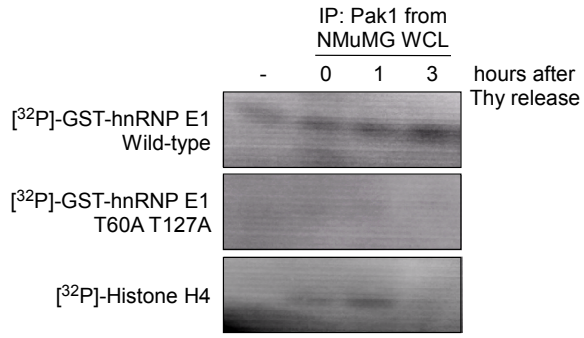

Figure 8: Pak1 phosphorylates recombinant hnRNP E1 *in vitro*.
Autoradiography images from *in vitro* kinase reactions. Pak1 was immunopurified from NMuMG cells synchronized at G1/S using double-thymidine block, then released for times indicated in the image. Incorporation of y-[^{32}P]-ATP into GST-hnRNP E1-WT, GST-hnRNP E1-phosphomutant (T60A T127A), and Histone H4 (control) are visualized.

The APC/C^{Cdh1} is impaired in E1KD cells as Cdh1 is constitutively degraded by the 26S proteasome. In order to determine whether constitutive expression of Cdc27 was affecting its normal function in the cell, we first assessed the expression level of APC/C substrates. Whole cell lysates were prepared from NMuMG and E1KD cells that had been synchronized at G0 as described previously. Lysates were resolved by SDS-PAGE and immunoblot analysis was performed. Plk1, a substrate of the APC/C bound to its cofactor Cdh1 (APC/C^{Cdh1}), is stabilized in E1KDs compared to NMuMGs (Fig. 9). Furthermore, expression of the APC/C^{Cdc20} substrate, securin, is diminished in E1KDs compared to NMuMGs (Fig. 9). The specificity of the APC/C for cyclin A remains unclear, and its expression level does not vary between NMuMG and E1KD cells (Fig. 9). The stabilization of Cdh1 substrates and decreased levels of Cdc20 substrates led us to look at expression levels of the cofactors themselves. Immunoblot analysis revealed that, indeed, the expression of Cdc20 is constitutively high in E1KDs, whereas Cdh1 is almost completely absent (Fig. 10A).

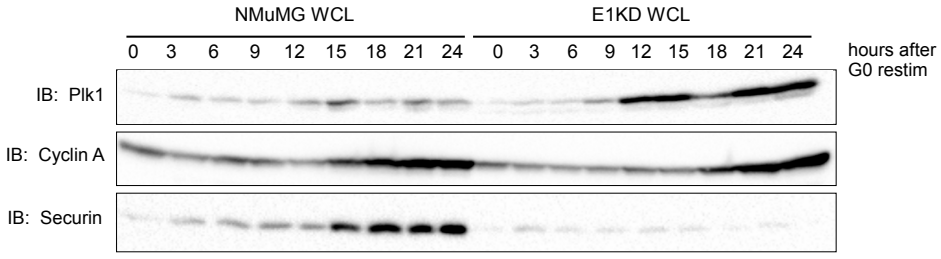

Figure 9: APC/C^{Cdh1} substrates are stabilized in E1KDs, while APC/C^{Cdc20} substrates are decreased. Immunoblot analysis of protein expression of Plk1, Cyclin A, and securin in whole cell lysates prepared from NMuMG and E1KD cells synchronized by overnight culturing in DMEM + 0.5% FBS, then release for times indicated in figure.

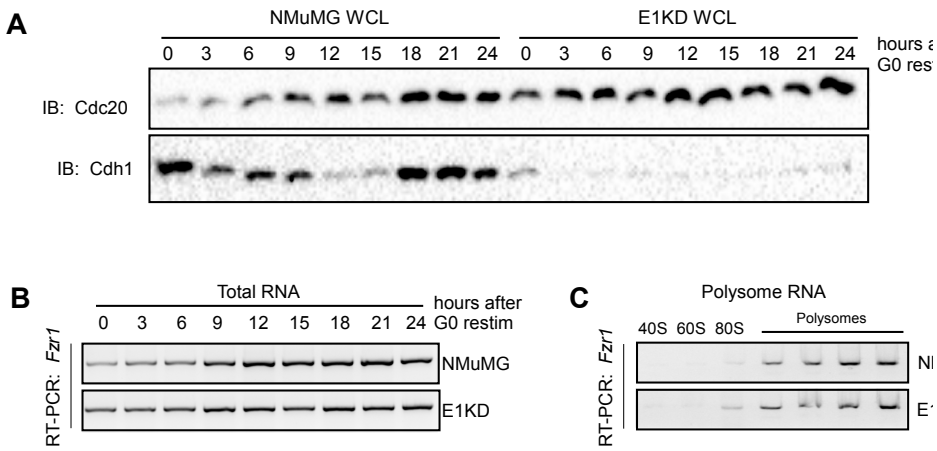

Figure 10: Cdh1 expression is lost in E1KDs. (A) Immunoblot analysis of expression of Cdc20 and Cdh1 in whole cell lysates prepared from G0-synchronized NMuMG and E1KD cells. (B) Semi-quantitative RT-PCR analysis with gene specific primers to *Fzr1* using total RNA isolated from G0-synchronized NMuMG and E1KD cells. (C) Semi-quantitative RT-PCR analysis using gene-specific primers to *Fzr1* using RNA isolated from polysome profiling of NMuMG and E1KD cytosolic extracts.

To determine the mechanism whereby Cdh1 expression is lost in E1KDs, we first assessed the levels of Cdh1 mRNA (gene name *Fzr1*). Total RNA was isolated from G0-synchronized NMuMG and E1KD cells, then reverse transcribed into cDNA using oligo-dT primers. Semiquantitative PCR was then performed using primers for *Fzr1*. Expression levels of *Fzr1* appear to be the same in E1KDs and NMuMGs (Fig. 10B).

To assess whether the *Fzr1* mRNA was being translated into protein, polysome profile analysis was repeated. Cytosolic extracts from NMuMG and E1KD cells were resolved on 10-50% sucrose gradients and total RNA was isolated from discrete fractions. The RNA was reverse-transcribed into cDNA, and then semi-quantitative PCR was performed to assess sedimentation of *Fzr1* mRNA. According to the results, *Fzr1* sediments to the heavy, polysomal fractions in both NMuMG and E1KD cells (Fig. 10C).

Finally, we wanted to investigate whether proteasomal degradation was responsible for the decreased levels of Cdh1 protein observed in E1KD cells. NMuMG and E1KD cells were treated with the 26S proteasome inhibitor, MG-132, at a concentration of 10 μM for 1 hour. Cdh1 expression was rescued in the E1KD cells treated with MG-132 (Fig. 11). Expression of hnRNP E1 is shown to validate the knockdown of hnRNP E1 in E1KD cells and GAPDH is shown as a loading control (Fig. 11).

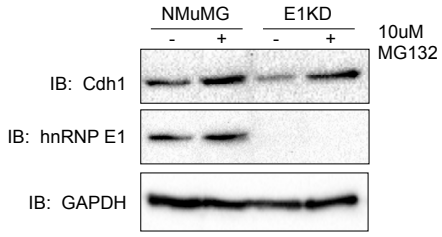

Figure 11: Cdh1 is proteasomally degraded in E1KD cells. Immunoblot analysis of protein expression in whole cell lysates prepared from NMuMG and E1KD cells treated -/+ 10 uM MG132 for 1 hour using anti-Cdh1, anti-hnRNP E1, and anti-GAPDH (control) antibodies.

The SCF E3 ubiquitin ligase bound to its cofactor, β-TRCP ($SCF^{\beta\text{-}TRCP}$) is responsible for canonical degradation of Cdh1during the cell cycle. To assess the activity of the SCF, we analyzed expression levels of its substrates. Briefly, cell lysates were prepared from NMuMG and E1KD cells that had been synchronized at G0 and re-stimulated. Lysates were resolved by SDS-PAGE, transferred to PVDF membrane, and immunoblot analysis was performed. β-catenin is a target of the $SCF^{\beta\text{-}TRCP}$, and its expression is markedly increased in E1KDs (Fig. 12). The cell cycle inhibitor, p27, is a target of the SCF bound to another cofactor, Skp2, and its expression is also elevated in E1KD cells (Fig. 12). The levels of both SCF cofactors, β-TRCP and Skp2, are decreased in E1KDs (Fig. 12).

The APC/C^{Cdc20} is constitutively active in E1KD cells and can ubiquitinate recombinant Cdh1 *in vitro*. Because other SCF substrates were not also being

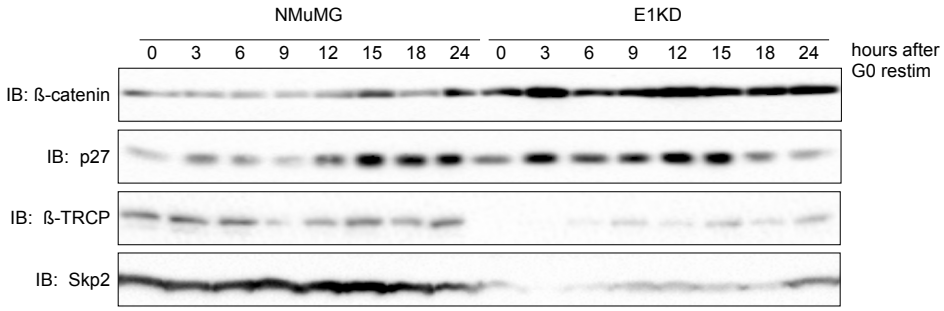

Figure 12: The ubiquitin ligase activity of the SCF is not elevated in E1KD cells. Immunoblot analysis of protein expression in whole cell lysates prepared from G0-synchronized and released NMuMG and E1KD cells using antibodies recognizing beta-Catenin, p27, beta-TRCP, and Skp2.

constitutively degraded in E1KD cells like Cdh1, we wanted to investigate the possibility that another E3 ubiquitin ligase could target Cdh1 in E1KDs. NMuMG and E1KD cells were treated with the APC/C inhibitor proTame for up to 6 hours and whole cell lysates were prepared at indicated time points (Fig. 13A). Lysates were resolved by SDS-PAGE and transferred to PVDF membrane. Immunoblot analysis was performed and the expression of Cdh1 appears to be rescued in E1KDs treated with proTame up to 3 hours. Both NMuMG and E1KD cells exhibit a decrease in Cdh1 at 6 hours of proTame treatment (Fig. 13A).

To determine whether the APC/C was responsible for Cdh1 degradation, *in vitro* ubiquitination assay was performed using APC/C affinity-purified from NMuMGs and E1KDs synchronized in either M phase or G1 phase using thymidine-nocodazole block and release, respectively. Cell extracts were prepared in ubiquitin lysis buffer and incubated with and α-Cdc16 antibody that had been conjugated to Protein G Sepharose beads. The immunopurified APC/C E3 ligase was then incubated with recombinant myc-tagged Cyclin B (residues 1-220) or recombinant GST-Cdh1 in the presence of E1-activating enzyme, E2-

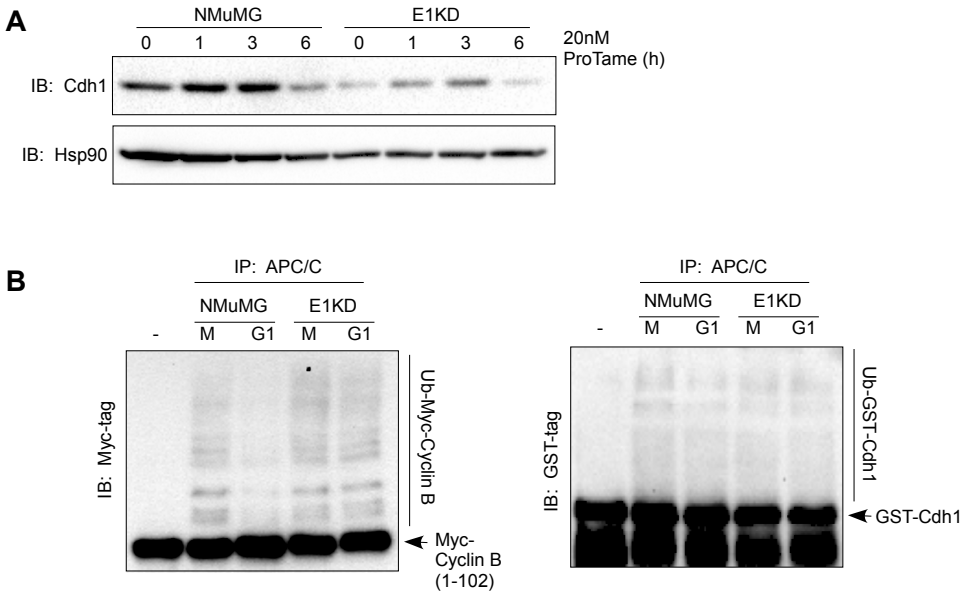

Figure 13: APC/C^{Cdc20} is constitutively active in E1KDs and can ubiquitinate GST-Cdh1 *in vitro*. (A) Immunoblot analysis of protein expression of Cdh1 and Hsp90 (control) in NMuMG and E1KD cells treated with the APC/C inhibitor proTAME for times indicated. (B) Immunoblot analysis of ubiquitination shifts of recombinant Myc-Cyclin B (residues 1-102) *left*, and GST-Cdh1 *right* resulting from *in vitro* ubiquitination reactions using APC/C immunopurified from mitotic and G1 NMuMG and E1KD cells, synchronized using thymidine-nocodazole block and release.

conjugating enzymes, and 1X ubiquitin reaction buffer. Reactions were stopped after 1 hour by addition of Laemmli sample buffer and then resolved by SDS-PAGE. After transferring to PVDF membrane, immunoblot analysis was performed using α-Myc tag antibody or α-GST tag antibody. Recombinant myc-tagged cyclin B was ubiquitinated by mitotic APC/C isolated from NMuMGs, and in both mitotic and G1 APC/C isolated from E1KD cells (Fig. 13B, left). Recombinant GST-Cdh1 was ubiquitinated by mitotic APC/C isolated from NMuMGs and by both G1 and mitotic APC/C isolated from E1KD cells (Fig. 13B, right).

In order to determine whether aberrant expression of Cdc27 was involved in premature activation of the APC/C^{Cdc20}, NMuMG cells were transfected with a plasmid expressing Flag-tagged Cdc27, now referred to as NMuMG-Cdc27 cells. Expression levels of Cdc27 are shown in NMuMG, E1KD, and NMuMG-Cdc27 cells and GAPDH was used as a loading control (Fig. 14A). NMuMG, E1KD, and NMuMG-Cdc27 cells were synchronized in mitosis using thymidine-nocodazole block, then released into G1. Cell lysates were prepared at indicated time points and resolved by SDS-PAGE. Immunoblot analysis of expression of Cdh1 in the three cell lines revealed that NMuMG-Cdc27 cells expressed Cdh1 at levels similar to E1KD cells (Fig. 14B). To confirm synchronization and exit from mitosis, levels of phosphorylated histone H3 are shown (Fig. 14B).

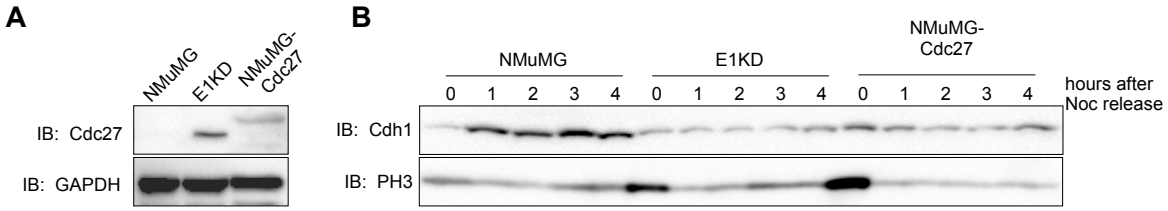

Figure 14: Overexpression of Cdc27 alone results in decreased levels of Cdh1. (A) Immunoblot analysis of Cdc27 and GAPDH (control) protein expression in NMuMG, E1KD, and NMuMG-Cdc27 cells. Flag-tagged Cdc27 is shifted up due to the molecular weight of the tag. (B) Immunoblot analysis of Cdh1 and phospho-histone H3 protein expression in NMuMG, E1KD, and NMuMG-Cdc27 whole cell lysates prepared from cells synchronized by thymidine-nocodazole block and release.

Loss of hnRNP E1 or overexpression of Cdc27 results in increased G2/M population and increased variability in chromosome number. E1KD-shCdc27 cells were developed in the laboratory and knockdown of Cdc27 expression is shown by immunoblot analysis of lysates prepared from NMuMG, E1KD, and E1KD-shCdc27 cells (Fig. 15A). To investigate the contribution of Cdc27 to cell cycle distribution, cell cycle

profile analyses of NMuMG, E1KD, NMuMG-Cdc27, and E1KD-shCdc27 cells were performed using propidium iodide staining of total cellular DNA followed by flow cytometric analysis. A larger percentage of E1KD and NMuMG-Cdc27 cells were found to be present in G2/M compared to NMuMGs and E1KD-shCdc27 cells (Fig. 15B).

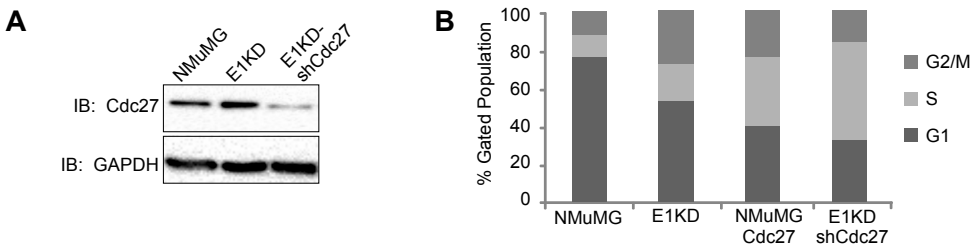

Figure 15: Modulating Cdc27 expression affects cell cycle distribution of NMuMG and E1KD cells. (A) Immunoblot analysis of Cdc27 and GAPDH (control) protein expression in NMuMG, E1KD, and E1KD-shCdc27 cells. (B) Cell cycle distribution analysis of NMuMG, E1KD, NMuMG-Cdc27, and E1KD-shCdc27 cells based on results of propidium iodide staining followed by flow cytometric measurement of cellular DNA content.

In order to further investigate the G2/M arrest observed in these cells, we performed immunofluorescent confocal microscopy of NMuMG, E1KD, and NMuMG-Cdc27 cells, staining for α-Tubulin, hnRNP E1, and DAPI (Fig. 16A). We observed many mitotic abnormalities such as metaphase plates with misaligned chromosomes and amplified centrosome numbers in E1KD and NMuMG-Cdc27 cells that were absent in the NMuMG control cells (Fig. 16B).

To determine whether the observed mitotic aberrations were giving rise to cells with aneuploid chromosome numbers, at least 50 metaphases from NMuMG, E1KD,

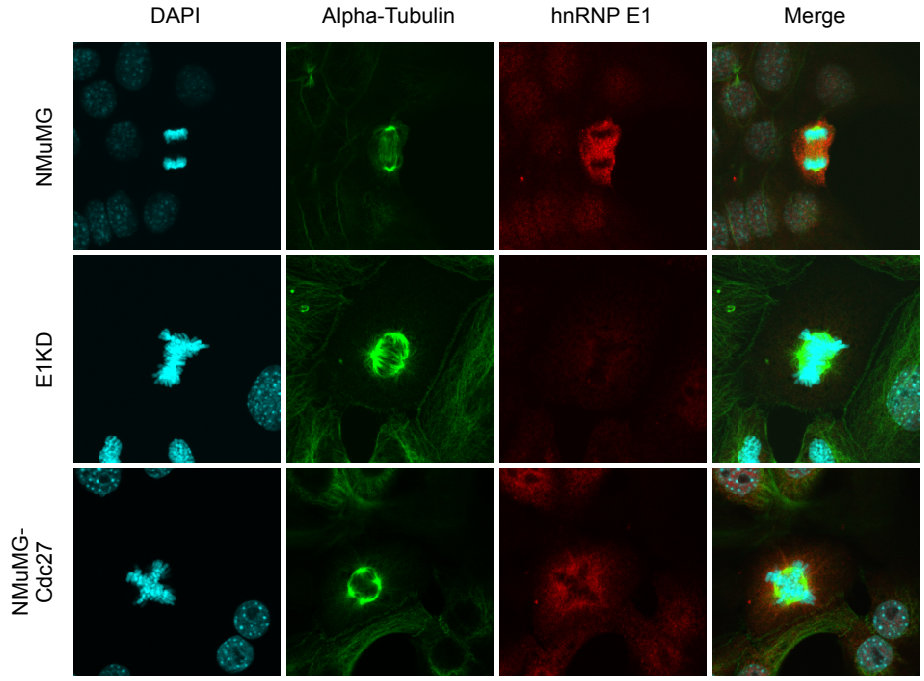

Figure 16: Mitotic aberrations occur in E1KD and NMuMG-Cdc27 cells. Immunofluorescence confocal microscopy images of representative mitoses of NMuMG, E1KD, and NMuMG-Cdc27 cells stained with DAPI (blue), alpha-Tubulin (green), and hnRNP E1 (red). Magnification is 120X.

NMuMG-Cdc27, and E1KD-shCdc27 cells were counted. Representative images of metaphase chromosome spread preparations stained with DAPI are shown on the left in Figure 5D. E1KD cells had significantly (P=0.032) higher numbers of aneuploid metaphases compared to NMuMGs as determined by unpaired Student's t-test (Fig. 17). Approximately 58% of NMuMG-Cdc27 metaphases counted had aneuploid chromosome numbers, however the data was not statistically significant when compared to NMuMG controls by unpaired Student's t-test (P=0.215). Finally, 72% of the E1KD-shCdc27 metaphases counted had aneuploid chromosome numbers.

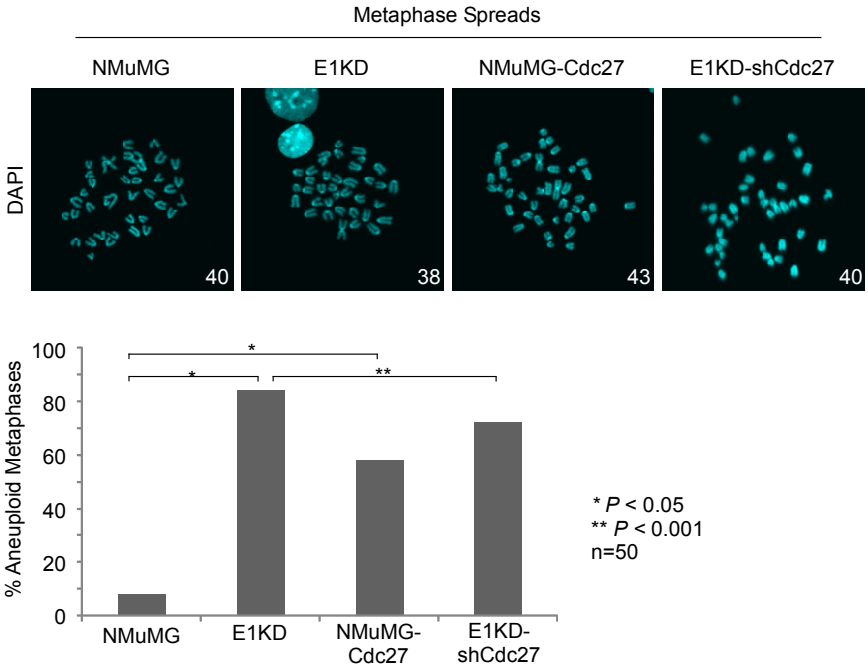

Figure 17: Modulating hnRNP E1 or Cdc27 expression induces chromosomal instability. Representative images of metaphase spreads prepared from NMuMG, E1KD, NMuMG-Cdc27, and E1KD-shCdc27 cells using DAPI to stain chromosomes. Magnification is 120X. Quantification of percent of aneuploid cells in populations. (n=50; Student's *t*-Test, * $P < 0.05$, ** $P < 0.001$)

Cdc27 is up regulated and Cdh1 is down regulated in *in vivo* selected metastasis model. The model describing the generation of *in vivo*-selected metastatic E1KD cells is shown in Figure 18. Characterization of the isolated cells *in vitro* revealed that L2P cells had the highest migratory (Fig. 19A) and invasive (Fig. 19B) phenotype compared to E1KD, M1P, and L1P cell lines as assessed by *in vitro* migration and *in vitro* invasion studies. Semi-quantitative RT-PCR analysis of NMuMG, E1KD, M1P, L1P, and L2P cells was performed to validate the identity of the cells isolated from mice using primers specific to

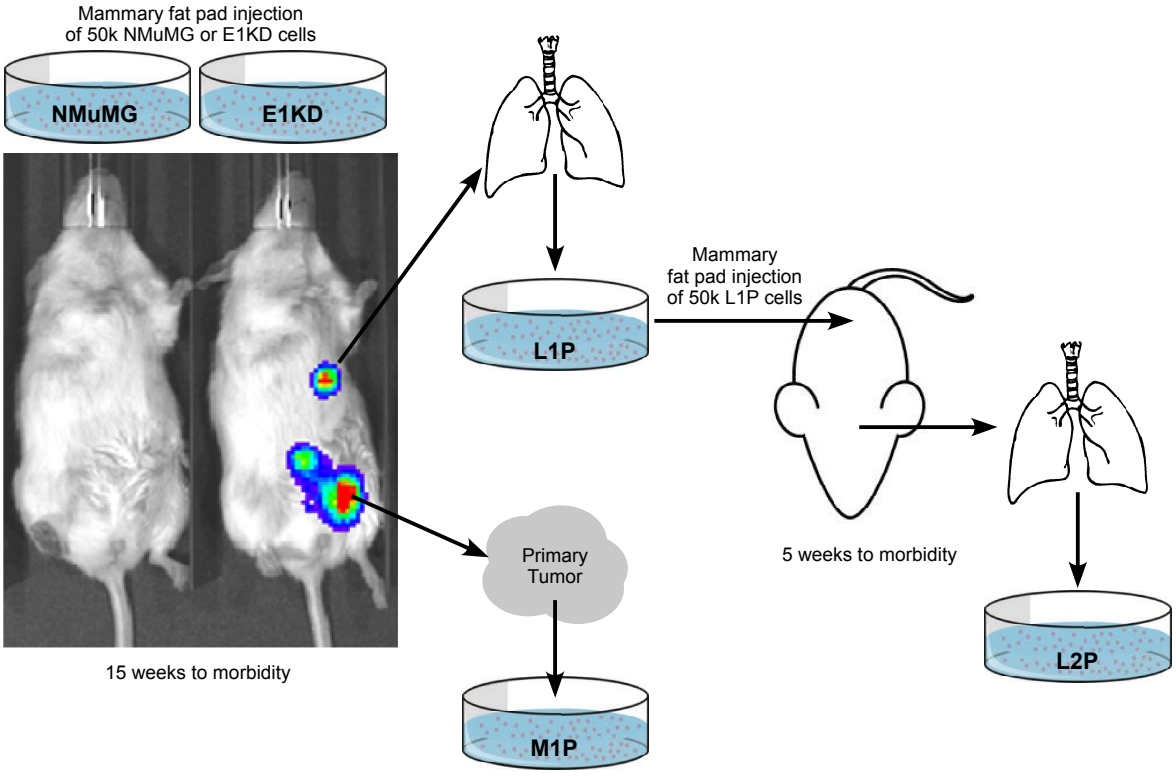

Figure 18: Model of E1KD Progression Series Isolation 50k E1KD cells were injected into the inguinal mammary fat pads of female NOD/SCID mice, then allowed to form tumors. Mice were euthanized at 15 weeks post-injection and primary tumors were enzymatically digested and cells cultured (M1P). Lungs were also enzymatically digested and grown in culture medium plus selection antibiotics (L1P). 50k L1P cells were injected into inguinal mammary fat pads of female NOD/SCID mice, allowed to form tumors, and mice were euthanized after 5 weeks due to significant morbidity. Lung metastases isolated from these mice were called L2P.

the sequence of the *pSilencer* plasmid and *Actb* was used as a loading control (Fig. 20). The process of *in vivo* selection of metastatic E1KD cells resulted in a slight increase in *Cdc27* mRNA expression and a large decrease in *Fzr1* mRNA expression (Fig. 20). The level of expression of Cdh1 protein was also decreased in M1P, L1P, and L2P cells compared to E1KD cells (Fig. 20).

***In vivo* selection of E1KD cells leads to a higher percentage of cells present in G2/M and a higher rate of aneuploidy.** Propidium iodide staining and flow cytometry

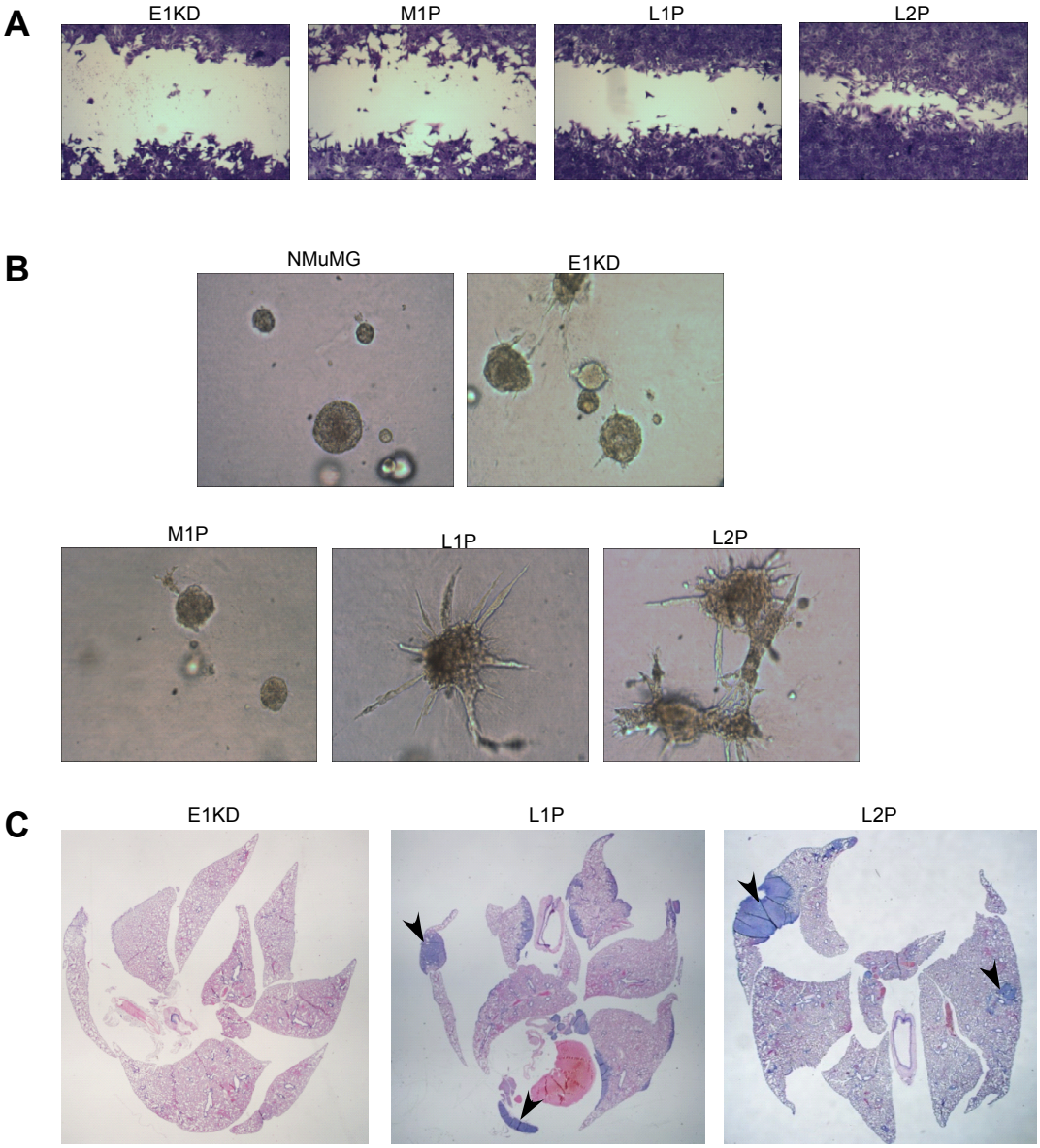

Figure 19: ***In vivo*** **passaging of E1KD cells results in increased migratory and invasive capability, as well as increased ability to colonize lung tissue.** (A) Representative image of stained and fixed cells following i*n vitro* migration assay using E1KD, M1P, L1P, and L2P. (B) Representative images of *in vitro* invasion assay using NMuMG, E1KD, M1P, L1P, and L2P cells. (C) Representative images of formalin-fixed paraffin-embedded lungs of NOD/SCID mice that had E1KD, L1P, or L2P cells injected via tail vein that have been stained using H&E. Arrows indicate metastatic lesions.

were performed using fixed NMuMG, E1KD, M1P, L1P, and L2P cells. The Dean-Jett model of DNA distribution was utilized to analyze cell cycle profiles of cell lines. G2/M populations of L1P and L2P cells were higher than NMuMG, E1KD, or M1P cells (Fig. 21A). Metaphase

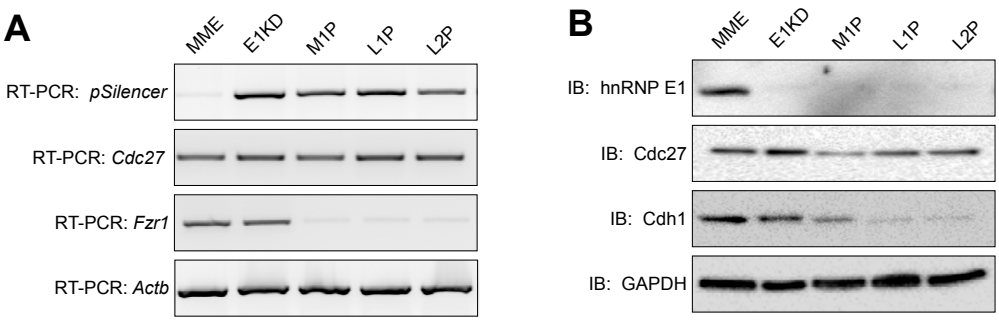

Figure 20: Validation of Identity of E1KD Progression Series Cells. (A) Semi-quantitative RT-PCR from total RNA isolated from NMuMG, E1KD, M1P, L1P, L2P cells using gene-specific primers to pSilencer plasmid, Cdc27, Fzr1, and Actb (control). (B) Immunoblot analysis of whole cell lysates isolated from NMuMG, E1KD, M1P, L1P, and L2P cells using antibodies recognizing hnRNP E1, Cdc27, Cdh1, and GAPDH (control).

spreads were prepared from M1P, L1P, and L2P cells and compared to NMuMG and E1KD spreads. Representative images of DAPI-stained metaphase spreads and average chromosome number ± S.E.M. are shown in Figure 20. L1P and L2P cells consistently exhibited a higher rate of aneuploidy than E1KD and M1P cells, resulting in a loss of 2 chromosomes for an average chromosome number of 38 (Fig. 21B).

High Cdc27 expression and high mitotic indices predict metastatic potential in breast cancer cell lines. In order to validate the significance of our findings in human disease, we first wanted to investigate expression of Cdc27 in normal human mammary epithelial cells and human breast cancer cell lines. Human mammary epithelial cells (HMLE) were used, as they contain two subpopulations of cells: a non-invasive, epithelial subtype (HMLE-epithelial) and a stably transitioned, mesenchymal subtype (HMLE-mesenchymal) that exhibit invasive and metastatic characteristics. We also developed hnRNP E1-knockdown HMLE-epithelial cells in our laboratory, termed HMLE-E1KD cells. Other breast cancer cell lines were also assayed, including MCF7, MDA-MB-231, MDA-MB-468, T47D, and BT-20. Whole cell lysates were prepared and resolved by SDS-PAGE.

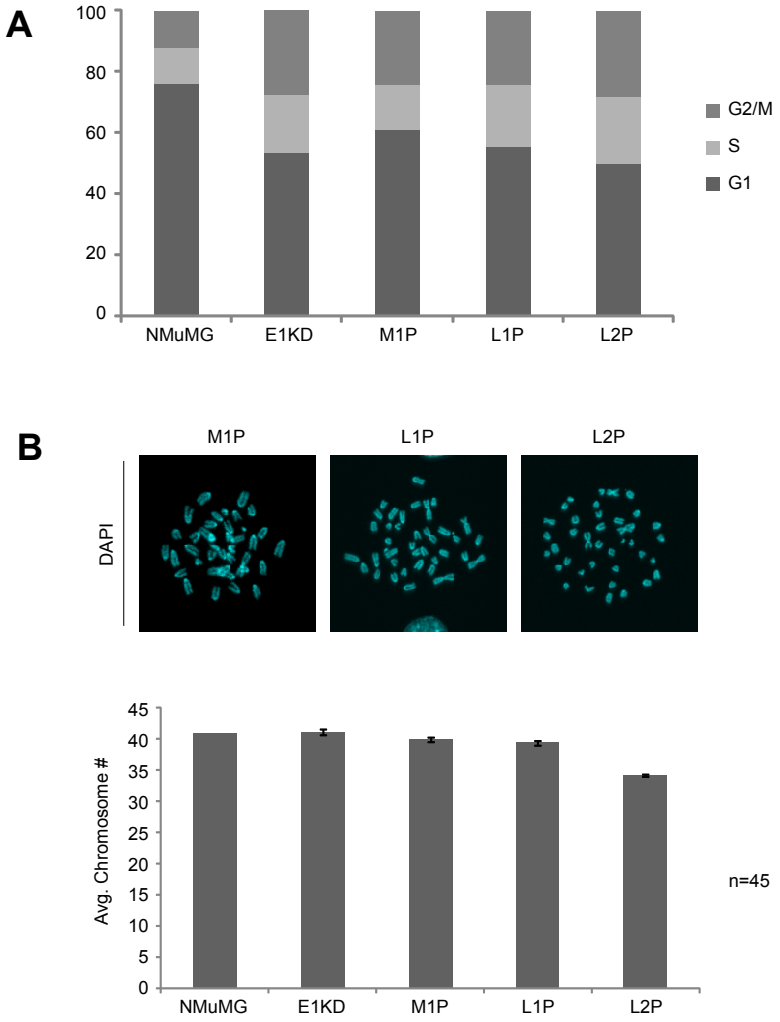

Figure 21: ***In vivo*** **selection results in increased G2/M population and increased aneuploidy.** (A) Cell cycle distributions of NMuMG, E1KD, M1P, L1P, and L2P cells based on propidium iodide staining followed by flow cytometric analysis. Percentages were calculated based on Dean-Jett mathematical model of DNA distribution. (B) Representative images of DAPI-stained metaphase spreads prepared from M1P, L1P, and L2P cells. Average chromosome counts are displayed -/+ S.E.M. 45 metaphases were counted per cell line.

Immunoblot analysis shows that both Cdc27 and Cdh1 expression is increased in the HMLE-mesenchymal and HMLE-E1KD cell lines compared to HMLE-epithelial cells; expression of hnRNP E1 is shown to validate the knockdown in HMLE-E1KD cells; GAPDH

is used as a loading control (Fig. 22A, left panels). Expression of Cdc27 and Cdh1 are highest in both MCF7 and MDA-MB-231 cells compared to MDA-MB-468, BT20, and T47D cells; hnRNP E1 expression is similar between all breast cancer cell lines and GAPDH expression is shown as a loading control (Fig. 22A, right panels).

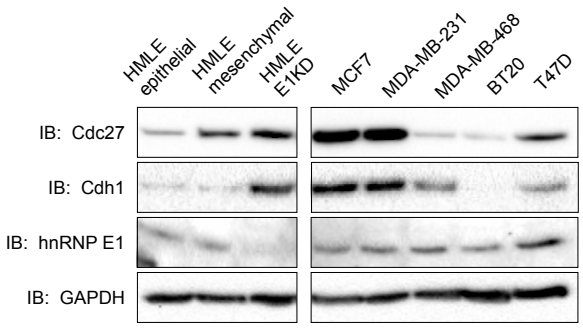

Figure 22: Cdc27 expression is increased in some breast cancer cell lines. Immunoblot analysis of protein expression in whole cell lysates isolated from breast cancer cell lines using antibodies recognizing Cdc27, Cdh1, hnRNP E1, and GAPDH (control).

Analysis of cell cycle distribution was performed using propidium iodide staining of total DNA followed by flow cytometry. HMLE-mesenchymal and HMLE-E1KD cells both had higher percentages of G2/M cells compared to HMLE-epithelial cells. MCF7 and MDA-MB-231 cells had the highest proportion of G2/M cells compared to other breast cancer cell lines. Finally, to quantify aneuploidy in breast cancer cell lines, metaphase spreads were prepared from cells and at least 35 metaphases were counted per cell line. Representative images of metaphases are shown in Figure 23. Results were quantified and presented as average chromosome count ± S.E.M. HMLE-epithelial cells were compared to HMLE-mesenchymal and HMLE-E1KD cells, and HMLE-mesenchymal cells exhibited significant aneuploidy compared to HMLE-epithelial cells, while HMLE-E1KD cells exhibited aneuploidy, but the data was not significant (Fig. 23, graph). MCF7, BT20, and T47D cell lines exhibited the highest amount of aneuploidy with chromosome numbers of approximately 3n (Fig. 23, graph).

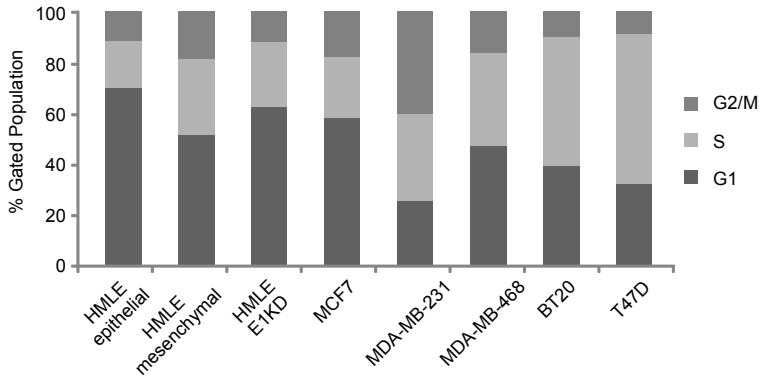

Figure 23: Percent of breast cancer cell line G2/M populations are highest in cell lines expressing highest levels of Cdc27. Cell cycle distributionsof breast cancer cell populations are shown, based on propidium iodide staining followed by flow cytometric analysis of total DNA content, corresponding to cell cycle phase.

Tissue microarray analysis of breast cancer patient samples reveals that high Cdc27 expression in tumor samples is a predictor of recurrence. Breast cancer patient tissue microarrays were assembled and stained for Cdc27 by the Hollings Cancer Center Tissue Biorepository as described above. A second investigator blinded to sample type and clinicopathological data performed independent scoring. Tissue sample staining was scored on a scale of 0 (low/negative staining) to 3 (intense staining). Significance was determined by Student's *t*-test. Scoring of TMA samples revealed that significantly ($P<0.001$) higher Cdc27 staining was present in tumor tissue compared to normal tissue (Fig. 24). Kaplan Meier survival analysis was performed using patient data provided and results indicated that high Cdc27 score significantly predicted a higher incidence of disease recurrence when compared to low Cdc27 score (Log rank $P = 0.046$) (Fig. 25).

Tissue microarray analysis was performed using Cdh1 antibody and the same breast cancer patient samples that were analyzed for Cdc27 expression. Expression of Cdh1 in breast cancer patient tumor tissue was significantly higher than in normal tissue ($P<0.001$) (Fig. 26A). In tumor lymph node samples, 5 out of 6 patients with low Cdh1 score

experienced disease recurrence, while only 2 out of 8 of those with high Cdh1 score experienced recurrence (Fig. 26B, Table 4).

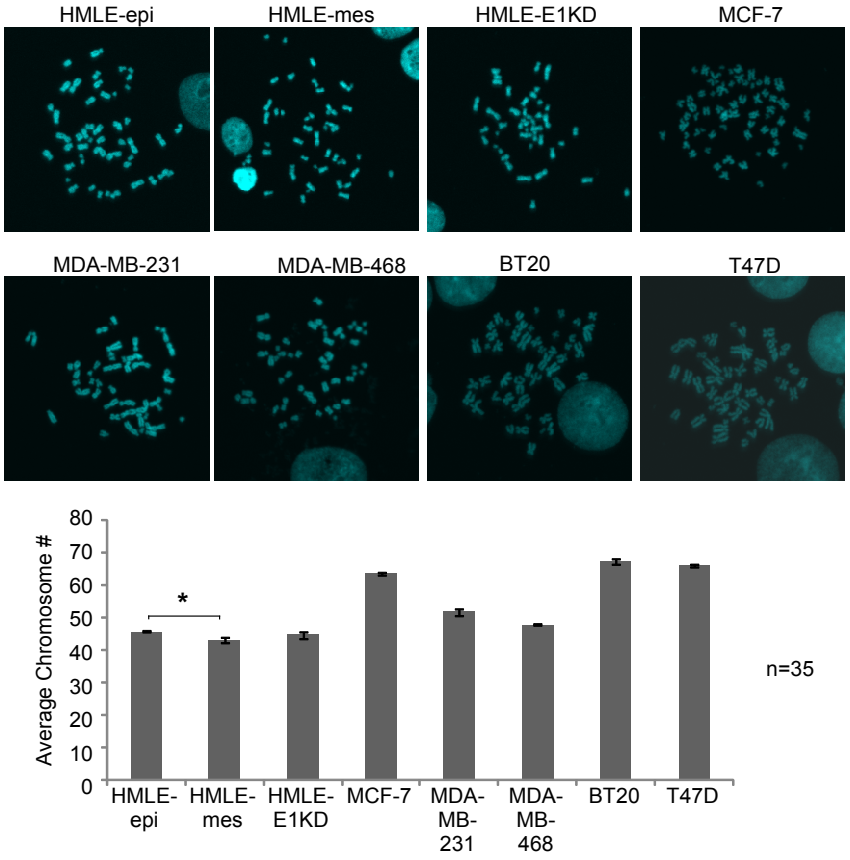

Figure 24: Breast cancer cell lines exhibit high amounts of aneuploidy. Representative images of metaphase spreads prepared from breast cancer cell lines using DAPI to stain chromosomes. Quantitation of average number of chromosomes -/+ SEM are shown below. (n=35; Student's *t*-Test, * $P < 0.05$)

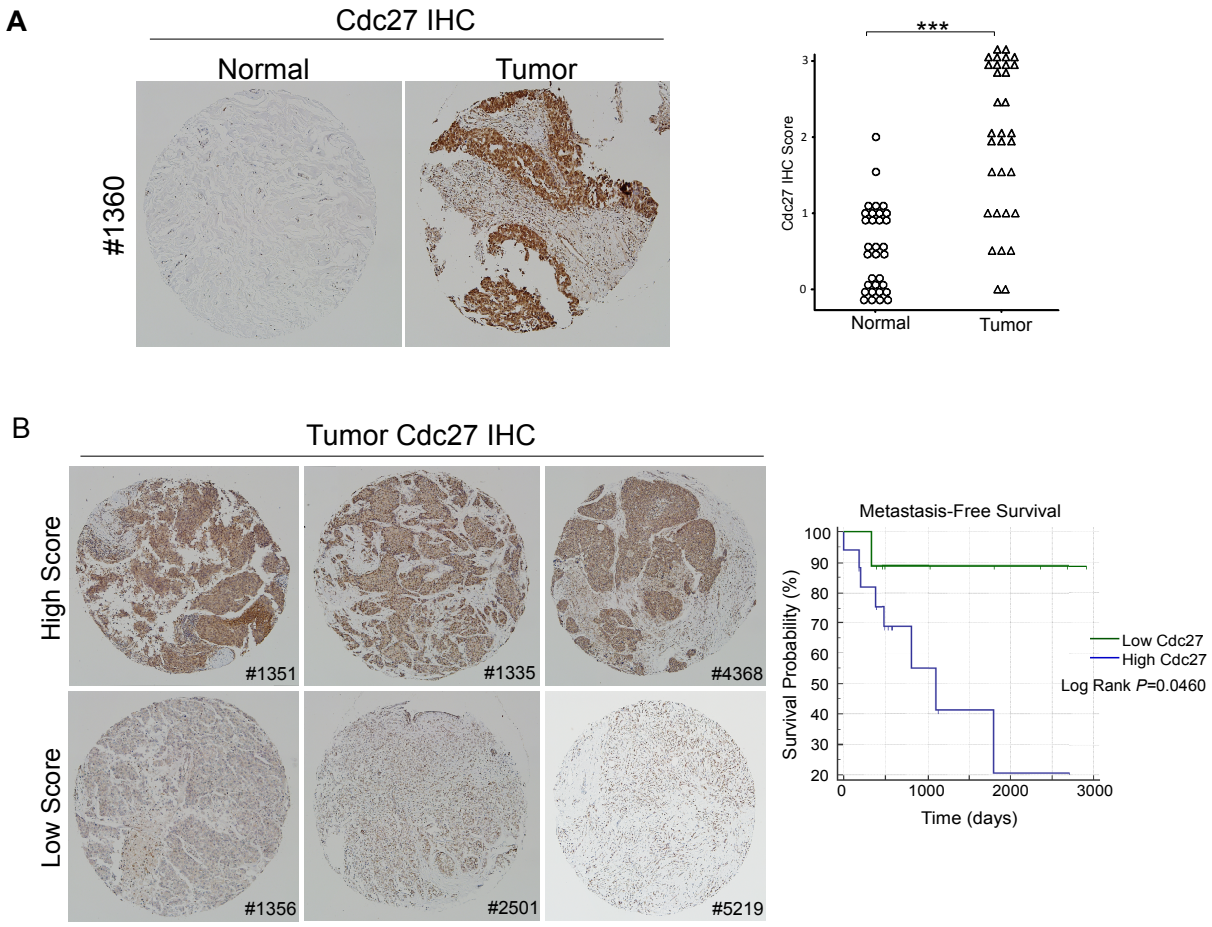

Figure 25: High Cdc27 score in breast cancer tumor patient samples significantly predicts recurrence of metastatic disease. (A) Representative images of immunohistological Cdc27 staining normal and tumor tissue isolated from breast cancer patients. Scoring of normal versus tumor is shown on the right (n=32; Student's *t*-Test, $P < 0.001$). (B) Representative images of high and low-score immunohistological Cdc27 staining in breast cancer patient tumor samples. Kaplan-Meier survival plot is shown on the right with High Cdc27 score significantly predicting disease recurrence (Log Rank $P < 0.05$).

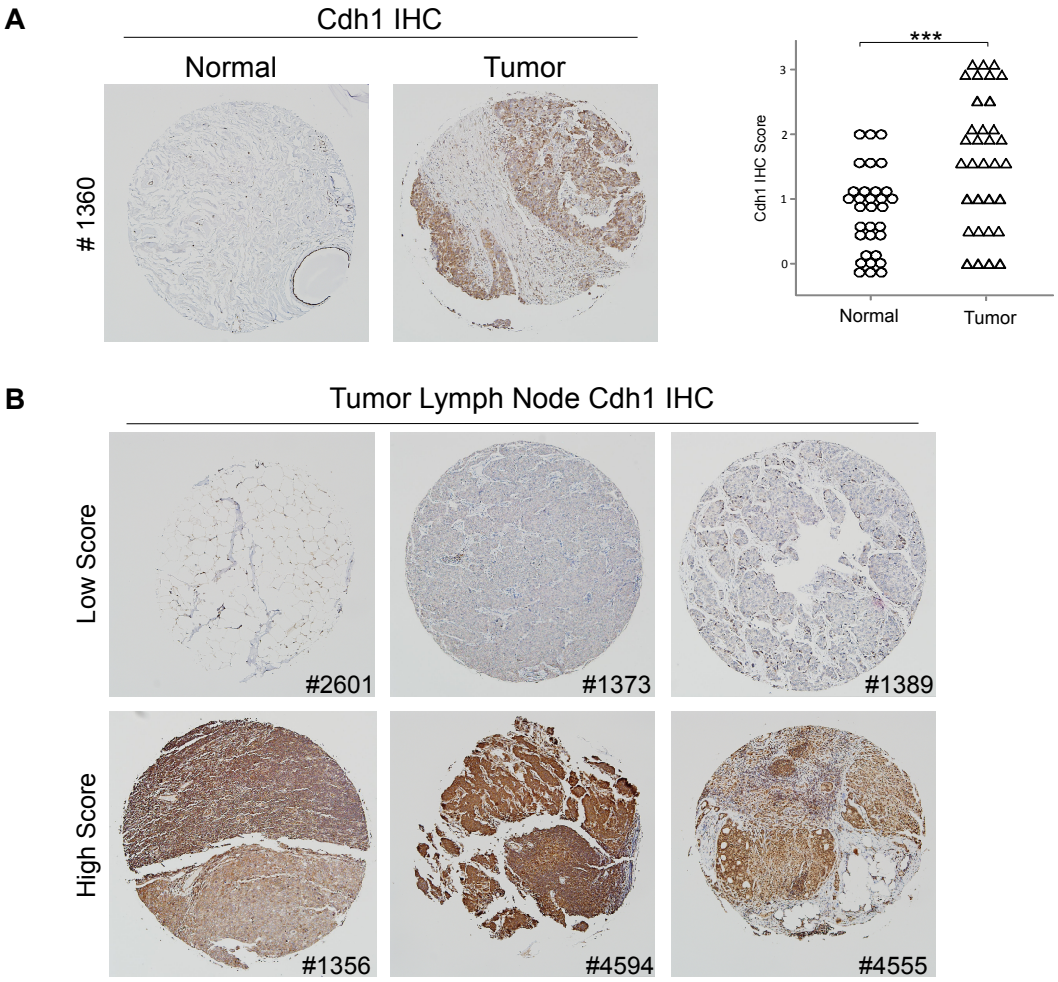

Figure 26: Cdh1 staining is signficantly higher in breast cancer patient tumor samples compared to normal. Representative images of Cdh1 immunohistological staining of tissue microarray samples from normal and tumor tissue isolated from breast cancer patients. Scoring of normal versus tumor is shown on the right. (n=33; Student's *t*-Test, $P < 0.001$). (B) Representative images of immunohistochemical staining of formalin-fixed paraffin-embedded tissue microarray samples from breast cancer patient tumor lymph nodes.

Patient	Vital Status	Recurrence	Days to Recurrence	Days to Death or Most Recent Contact
1335	Deceased	No		2713
1351	Alive	Yes	178	235
1356	Deceased	No		2916
1360	Alive	Yes	1802	2887
1373	Deceased	Yes	0 (prior surgery for ductal carcinoma in situ)	3022
1389	Deceased	Yes	806	2799
1420	Alive	Yes	373	474
1441	Deceased	No		2679
1459	Deceased	unknown		2666
1484	Alive	Yes	326	784
1773	Deceased	No		2365
1968	Alive	Yes	485	749
2501	Deceased	No		1811
2601	Alive	Yes	1101	1558
3565	Deceased	unknown		1312
4065	Deceased	unknown		1004
4215	Deceased	No		1132
4368	Deceased	No		1036
4555	Deceased	unknown		841
4594	Deceased	No		582
4673	Deceased	No		574
4684	Deceased	No		534
4692	Deceased	No		492
5010	Deceased	No		468
5076	Deceased	No		388
5108	Deceased	No		386
5116	Deceased	unknown		142
5126	Deceased	No		498
5219	Deceased	No		491
5317	Deceased	No		182
5428	Deceased	Yes		197
5615	Deceased	No		11

Table 2: Tissue Microarray Breast Cancer Patient Survival Data

Patient	Tumor Lymph Node Cdh1 Score	Recurrence
1335	Low	No
1373	Low	Yes
1389	Low	Yes
1420	Low	Yes
1968	Low	Yes
2601	Low	Yes
1351	High	Yes
1356	High	No
1484	High	Yes
4065	High	Unknown
4555	High	Unknown
4594	High	No
4692	High	No
5126	High	No

Table 3: Breast cancer patient tumor lymph node scoring and corresponding survival data. Low Cdh1 score in 83% of tumor lymph node samples was found to occur in patients who experienced metastatic recurrence, whereas high Cdh1 score in only 25% of tumor lymph node samples was found to occur in patients who experienced metastatic recurrence.

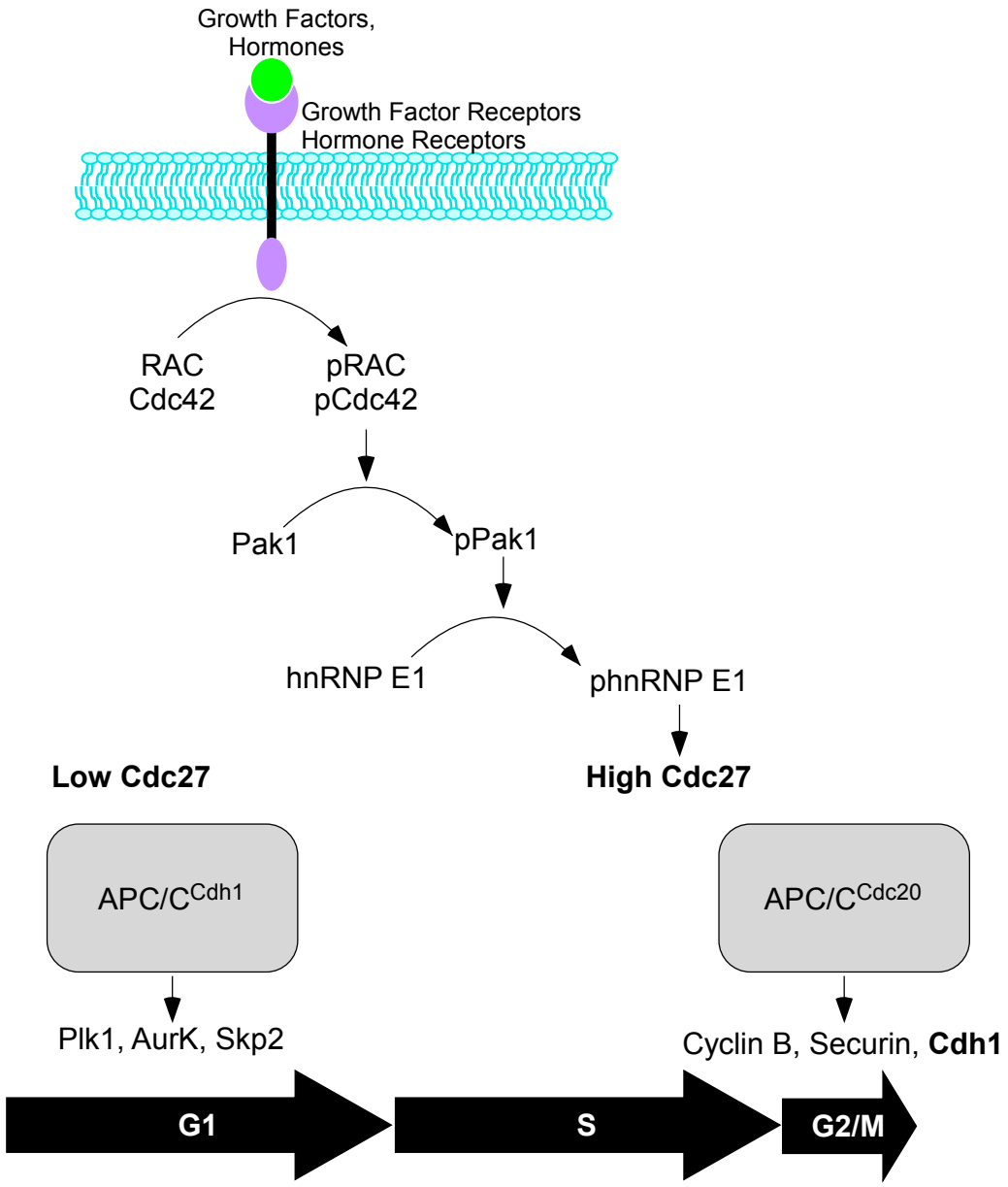

Figure 24: Model of hnRNP E1-mediated regulation of APC/C function through post-transcriptional regulation of Cdc27 expression. During G1, Cdc27 expression is low due to binding of hnRNP E1 to its mRNA. Activation of Rac/Cdc42 after the G1/S transition leads to phosphorylation and activation of Pak1, followed by phosphorylation of hnRNP E1 and its subsequent release from Cdc27 mRNA. Cdc27 expression is highest during mitosis, when APC/C-Cdc20 is active and APC/C^{Cdh1} is inactive. We hypothesize that APC/C^{Cdc20} regulates the levels of Cdh1 by ubiquitinating it, tagging it for 26S proteasome mediated degradation.

V. Chapter 5: Discussion

To elucidate other biological pathways in which hnRNP E1 is involved, the non-TGFβ-dependent transcripts identified were functionally annotated using DAVID Webtool (Dennis et al., 2003; Huang da, Sherman, & Lempicki, 2009) to determine whether any biological pathways were enriched in the gene set. The cutoff for change in expression between NMuMG monosomes and E1KD polysomes was 1.5-fold. Results of DAVID analysis are shown in Figure 1A. Nucleic acid metabolism was highly enriched, as well as cell cycle ($P<0.05$). It has been shown previously that hnRNP E1 is involved in mRNA transcription (Chaudhury, Chander, et al., 2010; Meng et al., 2007; Ostareck-Lederer et al., 1998; Xia et al., 2012), so its presence in the results of the analysis was expected.

We chose to further investigate the cell cycle genes that were translationally regulated by hnRNP E1. The loss of cell cycle regulation is one of the hallmarks of cancer progression (Hanahan & Weinberg, 2000, 2011). The consequences of defects in regulation of cell cycle include, but are not limited to, defective DNA damage repair, aneuploidy, proliferation in the absence of mitogenic stimulation, and insensitivity to anti-growth signaling (Hanahan & Weinberg, 2000, 2011), all of which have been attributed to the progression of cancer and metastasis. Within the group of hnRNP E1-regulated genes involved in cell cycle, we decided to further investigate *Cdc27* because of its role in the anaphase-promoting complex/cyclosome (APC/C). Cell division cycle 27 (Cdc27), also known as APC3, is a core component of the APC/C. During the cell cycle, the APC/C plays a critical role in facilitating the metaphase-to-anaphase transition, as well as preventing premature S-phase entry during G1 (Peters, 2002, 2006).

According to the model elucidated previously by our laboratory for hnRNP E1-mediated translational silencing (Chaudhury, Hussey, et al., 2010; Hussey et al., 2011), hnRNP E1 binds the 3'UTR of the mRNA as well as EF1A1 in the ribosomal A site. This interaction between hnRNP E1 and EF1A1 prevents the release of EF1A1 from the ribosome, stalling translation at the elongation step. The sedimentation of *Cdc27* mRNA to the 60S and 80S ribosomal fractions suggests that translation is initiating, but not occurring, possibly due to stalled elongation in the presence of hnRNP E1. There is some *Cdc27* present in the polysome fractions in NMuMG cells. This could be because *Cdc27* expression is dependent on cell cycle phase, and the cells used for this experiment were asynchronous. Those cells in later stages of the cell cycle are actively translating *Cdc27*, as I will show in the next figure. *Cdc27* mRNA is present primarily in the polysome fractions of E1KD cells (Fig. 2B). According to the model of hnRNP E1-mediated translational silencing, in the absence of hnRNP E1, *Cdc27* mRNA will be constitutively translated. The results support the model of hnRNP E1-mediated translational silencing. Translation of *Actb* is shown below *Cdc27* as a control to show that global translation is not increased in E1KD cells (Fig. 2B). The absorbance profiles of NMuMG and E1KD polysome analyses are shown below the PCR results to further provide evidence that global translation is similar between NMuMG and E1KD cells (Fig. 2B, lower).

Because of its role as a core component of a complex regulating cell cycle progression, we hypothesized that expression of Cdc27 might occur in a cell cycle-dependent manner in normal cells. Indeed, we found that Cdc27 expression increases at the protein level and not the transcript level during cell cycle progression, further

supporting the hypothesis that Cdc27 expression is regulated post-transcriptionally in the presence of hnRNP E1.

In order to show that Cdc27 expression is induced at the translational level after mitogenic stimulation, polysome profile analysis was performed using synchronized NMuMG and E1KD cells. In the G0-synchronized NMuMG cells (0h), *Cdc27* mRNA is present in the 60S and 80S fractions, corresponding to little or no translation. After re-stimulation with complete medium for 18 hours, *Cdc27* mRNA shifts to the polysomal fractions, suggesting an increased rate of translation (Fig. 5A). There is some *Cdc27* mRNA in the polysome fractions at 0h. This can be explained by the incomplete synchronization of the cell population by low serum. While nearly 75% of the cells are synchronized in G1 after overnight low serum-culture, some cells are still present in the later phases of the cell cycle. In the E1KD cells, *Cdc27* mRNA is present in the polysome fractions independent of cell cycle phase (Fig. 5A). This data suggests that *Cdc27* mRNA translation is both cell cycle- and hnRNP E1-dependent. Mitogenic signaling is sufficient to induce expression of Cdc27 at the protein level in NMuMGs.

The evidence for association between hnRNP E1 and Cdc27 up to this point has been indirect: the absence of hnRNP E1 leads to an increase in Cdc27 translation, independent of cell cycle phase. In order to determine whether hnRNP E1 was interacting directly with *Cdc27* mRNA, RNA immunoprecipitation was performed. NMuMG cells were synchronized using double thymidine block. This method was utilized instead of G0 synchronization for two reasons: first, it is highly effective at reversibly blocking a population of cells at the G1/S transition (Harper, 2005), and second, the increase in expression of Cdc27 protein in NMuMGs is observed shortly after the G1/S transition (Fig. 2A). According to the flow

cytometric analysis of cell cycle distribution shown in Figure 4, NMuMG cells enter S phase sometime between 12 and 18 hours after re-stimulation; synchronization at the G1/S transition eliminates the need for the first 12 hours of re-stimulation required by G0-synchronization. Based on the results of the RNA immunoprecipitation assay, hnRNP E1 protein binds *Cdc27* mRNA, and this interaction is abolished 3 hours after release from G1/S arrest (Fig. 5B). *L1CAM* mRNA is shown as a positive control, as others have shown previously that its translation is regulated by hnRNP E1 in a cell cycle-dependent manner (Meng et al., 2007). The interaction between *L1CAM* and *Cdc27* with hnRNP E1 follows the same pattern, suggesting that their interactions might be regulated by the same mechanism. *Actb* is included as a negative control, as it is not known to interact with hnRNP E1. As expected, hnRNP E1 does not immunoprecipitate *Actb* mRNA (Fig. 5B). Immunoprecipitations were also performed using IgG instead of α-hnRNP E1 antibody to ensure that the mRNA was not non-specifically associating with the Fc regions of the hnRNP E1 antibody. There was some non-specific immunoprecipitation of *Cdc27* mRNA in the IgG immunoprecipitation reactions, but it was very low compared to the hnRNP E1 immunoprecipitates and did not follow the same pattern of association, suggesting that the interactions observed in IgG immunoprecipitations are nonspecific. Input samples were obtained by isolating total RNA from cytosolic extracts and included to indicate that equal amounts of lysate and mRNA were present in all immunoprecipitation reactions.

The cell cycle-dependent loss of association between hnRNP E1 and *Cdc27* mRNA suggests that mitogenic signaling functions upstream of hnRNP E1, stimulating its release from *Cdc27* and allowing for Cdc27 protein expression. The interaction of *L1CAM* with hnRNP E1 follows the same pattern as *Cdc27*, suggesting that the two may be regulated by

the same mechanism. Meng et al. identified p21-activated kinase 1 (Pak1) as the kinase responsible for phosphorylating hnRNP E1 and causing its release from *L1CAM* mRNA, allowing for its translation (Meng et al., 2007). To investigate whether the same kinase was responsible for expression of Cdc27 during the cell cycle, we first wanted to determine whether mitogenic stimulation could result in hnRNP E1 phosphorylation, and also whether this phosphorylation was sensitive to the Pak1 inhibitor, IPA-3. IPA-3 is an allosteric inhibitor of Pak1 that covalently binds to the regulatory domain and prevents binding of its upstream activator, Cdc42 (Deacon et al., 2008; Viaud & Peterson, 2009). To investigate hnRNP E1 phosphorylation during the cell cycle, hnRNP E1 was immunoprecipitated from synchronized NMuMG whole cell lysates in the absence or presence of 30 μM IPA-3. The results reveal that hnRNP E1 is phosphorylated at 3 hours following release from G1/S arrest, and this phosphorylation event is absent in the presence of IPA-3 (Fig. 6A). The antibody used for immunoblot detection of phosphorylated hnRNP E1 is an HRP-conjugated antibody that recognizes the RXXS*/T* motif, where the serine or threonine with an asterisk is phosphorylated. Pak1 has been shown previously to phosphorylate residues on hnRNP E1: threonine 60 and threonine 127 (Chaudhury, Chander, et al., 2010; Meng et al., 2007). Both threonine residues have an arginine at their -3 positions, suggesting that this antibody can recognize Pak1-phosphorylated hnRNP E1. The inhibition of hnRNP E1 phosphorylation in the presence of IPA-3 as detected by this assay suggests that the antibody is recognizing Pak1-specific phosphorylation sites on hnRNP E1. The membrane was then stripped and re-probed for total hnRNP E1 using a different antibody than the one used for immunoprecipitation. The amount of hnRNP E1 immunoprecipitated at all time points was equal, indicating equal loading of lysate in

immunoprecipitation reactions and also indicating that total hnRNP E1 levels did not fluctuate during G1/S release or in the presence of IPA-3 (Fig. 6A).

Phosphorylation of hnRNP E1 has been shown previously to influence its ability to bind RNA (Chaudhury, Chander, et al., 2010; Ostareck et al., 1997; Ostareck-Lederer et al., 2002; Ostareck-Lederer et al., 1994). In this study, we hypothesize that the observed the loss of hnRNP E1 and *Cdc27* interaction results from Pak1-dependent hnRNP E1 phosphorylation, and this allows for translation of Cdc27. Immunoblot analysis of whole cell extracts that were G1/S-arrested and released reveals that Cdc27 expression is induced at around 3 hours post-G1/S release, coinciding with the observed phosphorylation of hnRNP E1 in Figure 3A (Fig. 6B). This increase in Cdc27 expression is not observed in the presence of the Pak1-specific inhibitor, IPA-3, and the expression of Cdc27 is constitutively high in E1KDs, irrespective of time or presence of IPA-3 (Fig. 6B). This suggests that Cdc27 translation is Pak1-dependent in NMuMG cells, while the absence of hnRNP E1 in E1KDs abrogates the need for Pak1-mediated hnRNP E1 phosphorylation to induce Cdc27 expression.

The whole cell extracts were further analyzed for Pak1 phosphorylation, which corresponds to its activation. The phosphorylation of Pak1 is at its highest 1 hour after G1/S release and is maintained at 3 hours (Fig. 6B). The kinase activity of Pak1 is itself regulated by phosphorylation, and it has many upstream kinases including Cdc42 and Rac (Maroto et al., 2008; Wang et al., 2006). Pak1 inhibition is evidenced by the lack of phospho-Pak1 in the IPA-3-treated NMuMG sample (Fig. 6B). In E1KD cells, the activation of Pak1 occurs in an almost identical fashion to the NMuMG cells and is inhibited in the IPA-3-treated sample (Fig. 6B). This suggests that Pak1 is activated in E1KDs during the cell

cycle and its activation is sensitive to IPA-3, however the absence of hnRNP E1 abrogates the need for this phosphorylation event to result in increased Cdc27 expression. GAPDH was included to ensure equal loading of cell lysate (Fig. 6B).

To further investigate the contribution of Pak1 to hnRNP E1-mediated translational silencing of *Cdc27*, RNA-immunoprecipitation was performed in the presence of IPA-3. NMuMG cells were synchronized at G1/S and released in the absence or presence of increasing concentrations of IPA-3. Semi-quantitative RT-PCR results reveal a decrease in interaction between hnRNP E1 protein and *Cdc27* mRNA at 3 hours post-G1/S-release (Fig. 7). This decrease in interaction is not observed in the presence of increasing concentrations of IPA-3 (Fig. 7). This data implies that, by inhibiting phosphorylation and subsequent activation of Pak1, Pak1-dependent phosphorylation of hnRNP E1 does not occur, resulting in its stabilization on *Cdc27* mRNA. Levels of *Cdc27* mRNA remain constant during release from G1/S and in the presence of IPA-3, as is evidenced by the input samples (Fig. 7). Immunoprecipitations with IgG were included as a control to show that *Cdc27* mRNA does not immunoprecipitate with the Fc portion of the α-hnRNP E1 antibody. There is some *Cdc27* mRNA present in the IgG immunoprecipitates, however it is much lower than the input and α-hnRNP E1 immunoprecipitation samples, indicating that the interaction is nonspecific (Fig. 7). *Actb* is included as it is not a known interacting partner of hnRNP E1, and results indicate that it does not immunoprecipitate with hnRNP or IgG (Fig. 7), further suggesting that the interaction between hnRNP E1 and *Cdc27* is specific.

Finally, we wanted to investigate whether immunopurified Pak1 from synchronized NMuMG cells could phosphorylate recombinant GST-hnRNP E1 *in vitro*. *In vitro* phosphorylation was performed by purifying Pak1 from NMuMG cell extracts that had been

arrested by double thymidine block and released, then incubating the immunopurified Pak1 with wild-type GST-hnRNP E1, a phospho-mutant GST-hnRNP E1 developed in the laboratory, or recombinant histone H4, a previously validated target of Pak1 phosphorylation (Maroto et al., 2008). The phosphomutant GST-hnRNP E1 was developed by sequential site-directed mutagenesis of the two known Pak1 phosphorylation sites in the wild-type plasmid. Primers were designed to mutate the DNA sequences coding for threonine 60 and threonine 127 in the wild-type GST-hnRNP E1 plasmid, converting them both to alanine in the new mutant plasmid. Mutation to alanine is an effective method in rendering an amino acid neutral to phosphorylation. The immunopurified kinase, recombinant substrate, and γ-[^{32}P]-ATP were incubated together, reactions were resolved by SDS-PAGE and then analyzed by autoradiography. According to the results, wild-type GST-hnRNP E1 and recombinant histone H4 are phosphorylated by immunopurified Pak1 *in vitro*, while the phospho-mutant GST-hnRNP E1 is not phosphorylated (Fig. 8). Furthermore, the highest level of phosphorylation of wild-type GST-hnRNP E1 occurs when incubating with the immunopurified Pak1 from NMuMGs that had been released from G1/S arrest for 3 hours, coinciding with the previous results for hnRNP E1 phosphorylation (Fig. 6A). These results suggest that the threonine 60 and threonine 127 residues of hnRNP E1 are necessary for Pak1-mediated hnRNP E1 phosphorylation. There is a small amount of phosphorylation of wild-type GST-hnRNP E1 in the absence of immunopurified kinase in the first lane of the autoradiography figure, however the phosphorylation is higher in the samples incubated with kinase and an increase in phosphorylation is apparent at 3 hours, indicating that this is likely background. The kinetics of recombinant histone H4 phosphorylation by immunopurified Pak1 are slightly different than those of wild-type

GST-hnRNP E1, however the initial increase in phosphorylation of both substrates occur at the same time, suggesting that there may be other modifications to Pak1 *in vivo* that affect its kinase activity with regard to histone H4.

We next wanted to investigate the impact that constitutively expressed Cdc27 had on E1KD cells. Because of its identity as a core component of the APC/C, our first goal was to determine whether the function of the APC/C was modulated in E1KDs compared to NMuMGs. The APC/C is an E3 ubiquitin ligase whose specificity relies on the presence of a cofactor, either Cdc20 or Cdh1 (Kramer et al., 2000; Peters, 2002, 2006; Visintin, Prinz, & Amon, 1997). The cofactor-dependent substrates of the APC/C are listed in Table 2. The APC/C^{Cdh1} is active primarily during late mitosis and through the G1 phase of the cell cycle, and one of its primary targets during late G1 is polo-like kinase 1 (Plk1) (Engelbert et al., 2008; Fukushima et al., 2013). The APC/C^{Cdh1} prevents premature S phase entry in late G1 by ubiquitinating Plk1, targeting it for proteolysis. There is another layer of regulation for Plk1, in that it is also regulated transcriptionally (Martin & Strebhardt, 2006). This double-layered regulation of Plk1 is important, as it is responsible for the phosphorylation-dependent degradation of Cdh1 for degradation by the SCF, another E3 ubiquitin ligase (Fukushima et al., 2013). Whole cell lysates from G0-synchronized NMuMG and E1KD cells were assayed by immunoblot to investigate the levels of Plk1. G0-synchronized lysates were utilized here in order to encompass a larger proportion of the cell cycle than double thymidine block allows, including early and late G1 phase during which APC/C^{Cdh1} is active. Levels of Plk1 are markedly increased in the E1KD cells in late G1, suggesting stabilization of the protein and possibly decreased function of the APC/C^{Cdh1} (Fig. 9). Expression of *Plk1* transcript were assayed and found to be the same between NMuMG and E1KD cells (data

not shown). The mechanism by which APC/C^{Cdc20} targets Cyclin A has been debated (Brito & Rieder, 2006; Izawa & Pines, 2011; Kramer et al., 2000; Prosser et al., 2012), and its expression is consistent in NMuMG and E1KDs (Fig. 9). Expression of securin, a target of APC/C^{Cdc20}, is largely diminished in E1KD cells compared to NMuMGs, suggesting possible hyperactivation of the APC/C^{Cdc20} in these cells (Fig. 9). Securin functions to bind and sequester the enzyme separase, preventing separase-mediated cleavage of cohesin rings that tether sister chromatids together at the metaphase plate prior to anaphase. After the mitotic checkpoint has been satisfied and inactivated, the APC/C^{Cdc20} is activated and ubiquitinates securin, causing the release of separase and the subsequent initiation of anaphase (Izawa & Pines, 2011; Peters, 2002; Visintin et al., 1997). The stabilization of an APC/C^{Cdh1} substrate and loss of an APC/C^{Cdc20} substrate in E1KDs indicated that the activity of the APC/C might be deregulated.

APC/C^{Cdh1} Substrates	APC/C^{Cdc20} Substrates
Plk1, Skp2, aurora kinases, Cdc20, geminin, Cyclin A	Cyclin B, securin

Table 4: Cofactor-specific APC/C substrates

To assess the expression levels of the cofactors Cdc20 and Cdh1, immunoblot analysis was performed on whole cell lysates of G0-synchronized NMuMG and E1KDs. The results showed that, while Cdc20 expression was high throughout the cell cycle in E1KDs, Cdh1 expression was almost completely absent (Fig. 10A). The absence of Cdh1 could explain the stabilization of the APC/C^{Cdh1} substrate, Plk1. Furthermore, the increased expression of Cdc20 could explain the destabilization of APC/C^{Cdc20} substrate, securin. This

result was interesting, because others have shown that Cdh1 is necessary for maintenance of chromosomal integrity and is a putative tumor suppressor (Engelbert et al., 2008; Fukushima et al., 2013; Garcia-Higuera et al., 2008; Listovsky & Sale, 2013). Because Cdh1 had been shown to be an important contributor to chromosomal integrity and prevention of unscheduled proliferation, we wanted to further investigate the mechanism by which its expression was lost in E1KDs. The expression of *Fzr1* at the mRNA level remained unchanged between NMuMG and E1KD cells (Fig. 10B), suggesting that its decreased expression occurred post-transcriptionally. Furthermore, polysome profile analysis of *Fzr1* indicated that its mRNA was being translated, as it sedimented to polysome fractions in both NMuMG and E1KD cells (Fig. 10C). This result provided evidence that *Fzr1* was being transcribed and translated, and so suggested that the decreased expression observed in E1KD cells could be due to increased degradation. The proteasomal inhibitor MG132 was used to ascertain whether proteasomal degradation was responsible for the decreased levels of Cdh1 in E1KDs. MG132 is a peptide aldehyde that prevents the 26S proteasome from degrading ubiquitinated proteins (Lee & Goldberg, 1998). Cdh1 expression was increased slightly in NMuMG and increased markedly E1KD cells treated for 1 hour with 10 μM MG132 (Fig. 11). The rescue of Cdh1 protein in E1KDs in the presence of MG132 provided evidence that proteasomal degradation was eliminating the transcribed and translated Cdh1 in the cells.

Proteasome-mediated degradation of Cdh1 occurs normally during the cell cycle. Near the end of G1 phase, Cdh1 is sequentially phosphorylated by cyclin dependent kinase 2 and then Plk1, resulting in its release from the APC/C core complex and subsequent recognition by the SCF, another E3 ubiquitin ligase (Fukushima et al., 2013). Ubiquitinated

Cdh1 is the recognized by the 26S proteasome and degraded. We were interested in determining whether the activity of the SCF was modulated in E1KDs, thus potentially resulting in increased ubiquitination and degradation of Cdh1. The SCF, much like the APC/C, regulates its specificity by the presence of a cofactor: β-TRCP or Skp2 (Benmaamar & Pagano, 2005; Fukushima et al., 2013; Kurland & Tansey, 2004). The $SCF^{\beta\text{-}TRCP}$ specifically recognizes phosphorylated Cdh1, ubiquitinating it and tagging it for proteasomal destruction (Benmaamar & Pagano, 2005; Fukushima et al., 2013). To assess SCF functionality, levels of substrate-specific SCF substrates were analyzed in NMuMG and E1KDs. Immunoblot analysis showed that the $SCF^{\beta\text{-}TRCP}$ substrate β-catenin was increased in E1KDs (Fig. 12). Importantly, this evidence implies that activity of the $SCF^{\beta\text{-}TRCP}$ is not enhanced in E1KDs with regard to other substrates, potentially ruling out the SCF as the responsible party in Cdh1 degradation. The observed increase in β-catenin could be a result of increased Wnt signaling in E1KD cells. The SCF^{Skp2} substrate p27 was also increased in E1KDs (Fig. 12). This result was not initially expected, since p27 functions as an inhibitor of the cell cycle, however recently it has been shown that p27 can function dually as both an inhibitor and promoter of CDK function (Chu, Hengst, & Slingerland, 2008; Moller, 2000). Nevertheless, the increase in p27 expression indicates that SCF^{Skp2} E3 ligase activity is also not increased in E1KDs. The expression levels of β-TRCP and Skp2 were also assessed in NMuMG and E1KD cells, revealing decreased levels of both SCF cofactors (Fig. 12). The previously found increases in β-catenin and p27 expression in E1KDs may result from this decrease in levels of SCF cofactors. While this result was interesting, it could not explain the increase in Cdh1 degradation. If the $SCF^{\beta TRCP}$ was constitutively active, one would expect its other substrates to be degraded as well. To this

point, the results suggest that Cdh1 is being proteasomally degraded in E1KDs and that increased $SCF^{\beta TRCP}$ activity was not responsible. We considered another potential explanation for increased Cdh1 degradation in E1KDs: constitutive phosphorylation of Cdh1 by Plk1. This was an attractive explanation since Plk1, one of the kinases responsible for Cdh1 phosphorylation and subsequent ubiquitination by the SCF, was found to be up regulated in E1KDs. However, Plk1 is absent in early G1 in both NMuMGs and E1KDs (Fig. 9). If Plk1-mediated phosphorylation of Cdh1 were responsible for its ubiquitination and degradation in E1KDs, we would still expect to detect Cdh1 during early G1 when Plk1 is absent. This is not the case, further suggesting that Cdh1 degradation in E1KDs is not due to increased Plk1 phosphorylation.

Earlier experiments suggested that the APC/C^{Cdc20} was prematurely activated in E1KDs, as evidenced by the lack of securin expression (Fig. 9). We hypothesized that a constitutively active APC/C^{Cdc20} could ubiquitinate and degrade Cdh1. APC/C-mediated Cdh1 degradation has been reported previously, however it was reported that APC/C^{Cdh1} self-ubiquitinates Cdh1 (Listovsky et al., 2004; Pfleger & Kirschner, 2000). It has not been shown previously that APC/C^{Cdc20} recognizes and ubiquitinates Cdh1. In order to investigate the contribution of the APC/C to Cdh1 degradation in E1KDs, the APC/C inhibitor proTAME was used. ProTAME is a pro-drug that is converted to its mature form, TAME, by intracellular esterases and functions by inhibiting activation of the APC/C by either Cdc20 or Cdh1 (Zeng & King, 2012; Zeng et al., 2010). NMuMG and E1KD cells were treated with proTAME for up to 6 hours and a slight increase in Cdh1 protein can be observed in NMuMGs, while a more obvious increase is seen in E1KDs (Fig. 13A). The level of Cdh1 is decreased in both NMuMG and E1KD cells at 6 hours, however we believe that

this is due to cytotoxicity, as the level of Hsp90, used as a protein loading control, is also decreasing with proTAME treatment. These results indicate that, since inhibition of APC/C in E1KDs resulted in an increase in the amount of Cdh1, Cdh1 is being targeted by the APC/C. This could be a direct result of APC/C-mediated ubiquitin ligation, or the result of stabilization of another APC/C target that protects Cdh1 stability. The rescue of Cdh1 by proTAME and by MG132 both occurred within 1 hour of treatment, suggesting that an intermediate does not exist between APC/C-mediated ubiquitination and 26S proteasome-mediated degradation. However, the results thus far could not rule out an intermediate as a possibility, so the direct activity of the APC/C was assessed *in vitro*.

We performed *in vitro* ubiquitination analysis with immunopurified mitotic- or G1-APC/C from NMuMG and E1KD cells and recombinant substrates. Cells were synchronized in mitosis using thymidine block followed by release into nocodazole. After 12 hours of incubation in nocodazole, cells were released into G1. As evidence of the activity of APC/C in normal, untransformed cells, we showed that mitotic-APC/C from NMuMGs was able to ubiquitinate recombinant myc-tagged cyclin B *in vitro* while G1-APC/C did not (Fig. 13B). Interestingly, both mitotic- and G1-APC/C isolated from E1KD cells was capable of ubiquitinating recombinant myc-tagged cyclin B *in vitro* (Fig. 13B, left panel), suggesting that the APC/C^{Cdc20} is constitutively active in E1KDs. This observation agrees with the earlier finding that the APC/C^{Cdc20} target, securin, is absent in E1KDs throughout the cell cycle (Fig. 9). We then investigated whether mitotic or G1-APC/C could ubiquitinate recombinant GST-Cdh1 *in vitro*. Results indicate that mitotic-APC/C isolated from NMuMG cells is capable of ubiquitinating Cdh1 more efficiently than G1-APC/C based on the amount of shifted Ub-GST-Cdh1 (Fig. 13B, right panel). Both mitotic- and G1-APC/C isolated from

E1KD cells ubiquitinate GST-Cdh1 with approximately the same efficiency, based on the amount of shifted Ub-GST-Cdh1 in both lanes (Fig. 13B, right panel). Overall, the results of the *in vitro* ubiquitination assays suggest two things: first, the APC/C^{Cdc20} is constitutively active in E1KD cells, and second, the mitotic APC/C is capable of ubiquitinating Cdh1.

We then wanted to address the question of whether excess Cdc27 could facilitate premature activation of the APC/C^{Cdc20}. In order to assess the effect of Cdc27 alone, a plasmid expressing Flag-tagged Cdc27 open reading frame was stably transfected into NMuMG cells, which we named NMuMG-Cdc27. Immunoblot analysis of Cdc27 expression in NMuMG, E1KD, and NMuMG-Cdc27 cells is shown in Figure 5C. The Flag-tagged Cdc27 is detected at a slightly higher molecular weight than endogenous Cdc27 because of the additional weight of the Flag tag. GAPDH is included as a loading control (Fig. 14A). Next, we were interested in determining whether expressing Cdc27 alone in NMuMG cells was sufficient to induce degradation of Cdh1. NMuMG, E1KD, and NMuMG-Cdc27 cells were synchronized at mitosis by thymidine-nocodazole block, then released into G1 phase. Blocking in mitosis would allow us to see the activity of the APC/C^{Cdc20}, as well as that of the APC/C^{Cdh1} in early G1 phase. In both the E1KD and NMuMG-Cdc27 cells, Cdh1 expression is not restored after release from mitotic arrest, whereas it does increase in the NMuMGs (Fig. 14B). Immunoblot analysis also included levels of phosphorylated histone H3, a marker that is commonly used to indicate presence in mitosis. Based on these results, it appears that all three cell lines are able to exit mitosis, however levels of Cdh1 are not restored in the G1 phase of E1KD or NMuMG-Cdc27 cells. Further analysis is necessary to validate the premature activation of the APC/C^{Cdc20} in NMuMG-Cdc27 cells, including *in*

vitro ubiquitination assay and analysis of the expression of other APC/C substrates such as securin and Plk1.

According to our results, Cdc27 expression is normally low during the G1 phase of the cell cycle, and then it is induced after the G1/S transition by Pak1-mediated phosphorylation of hnRNP E1. This increase in Cdc27 expression coincides with the observed decrease in Cdh1 expression, implying that there may be a relationship between increased Cdc27 expression and decreased Cdh1 expression in normal cells. The exact molecular mechanism underlying the premature activation of the APC/C^{Cdc20} in E1KD cells remains unclear, however a direct role for Cdc27 is suggested by the constitutive degradation of Cdh1 in NMuMG-Cdc27 cells. We intend to further investigate the contribution of Cdc27 to the degradation of Cdh1 by *in vitro* ubiquitination using APC/C isolated from NMuMG-Cdc27 cells and also Cdc20 knockdown studies in E1KD cells.

The anaphase-promoting complex/cyclosome is named for its function in promoting the metaphase-to-anaphase transition, wherein cells divide their duplicated genetic material prior to cell division. Premature activation of the APC/C has been implicated in cancer, especially in the acquisition of aneuploidy (Listovsky & Sale, 2013; Prosser et al., 2012). One consequence of premature activation of the APC/C^{Cdc20} or loss of Cdh1 is a decrease in the percentage of cells present in the G1 phase of the cell cycle, as APC/C^{Cdh1} functions to prevent early S phase entry under normal conditions (Sigl et al., 2009). We investigated whether silencing hnRNP E1 or expressing exogenous Cdc27 had an effect on the cell cycle distributions of NMuMG, E1KD, NMuMG-Cdc27, and E1KD-shCdc27 cells. E1KD-shCdc27 cells were generated in the laboratory by lentiviral shRNA transduction and the level of knockdown is shown by immunoblot assay in Figure 15A. GAPDH is included as

a loading control. To analyze cell cycle distribution, propidium iodide staining of total genomic DNA was performed in fixed NMuMG, E1KD, NMuMG-Cdc27 and E1KD-shCdc27 cells followed by flow cytometric analysis of DNA content. The percentage of cells in G1 phase in E1KD and NMuMG-Cdc27 populations is decreased when compared to NMuMG parental cell population. The percentage of E1KD-shCdc27 population in G1 phase is decreased compared to E1KDs (Fig. 15B). These results imply that hnRNP E1, through translational regulation of Cdc27, plays a role in maintaining G1 phase in NMuMG cells. It also strongly implies a role for Cdc27 alone in maintenance of G1 phase.

Premature activation of the APC/C has other consequences, including mitotic aberrations that are caused by the initiation of anaphase prior to proper chromosomal alignment at the metaphase plate and microtubule attachment (Prosser et al., 2012). Interestingly, the percentage of cells present in G2/M in the E1KD and NMuMG-Cdc27 cell populations was found to be increased compared to NMuMG cells (Fig. 6B), suggesting G2/M arrest or prolonged mitoses. In order to determine whether mitotic aberrations were occurring in cells with excess Cdc27, immunocytochemistry was performed on NMuMG, E1KD, and NMuMG-Cdc27 cells. Cells were fixed and stained with antibodies recognizing alpha-tubulin, hnRNP E1, and DAPI was used to stain DNA. Confocal immunofluorescent microscopy was performed to image cells in various stages of mitosis. Representative images are shown in Figure 16. While NMuMG cells underwent normal mitoses with properly aligned chromosomes in metaphase and normal anaphases, E1KD and NMuMG-Cdc27 cells exhibited several mitotic aberrations, especially centrosome amplification (Fig. 16). Others have shown that prolonged mitotic arrest as a result of loss of Cdh1 has been implicated in centrosome amplification (Anderhub, Kramer, & Maier, 2012; Prosser et al.,

2012). The total number of mitotic cells comprised a low percentage of the total number of cells imaged, so the percentage of cells with mitotic aberrations in E1KD and NMuMG-Cdc27 cells was not statistically significant. In an attempt to increase the proportion of mitotic cells in each cell population, nocodazole was used and unsuccessful, since its microtubule-destabilizing properties induced a large number of mitotic aberrations in all cells. In an effort to quantify the effects of the mitotic aberrations observed in NMuMG-Cdc27 and E1KD cells, metaphase spreads were prepared and chromosomes were counted. Representative images of metaphase spreads of NMuMG, E1KD, NMuMG-Cdc27, and E1KD-shCdc27 cells are shown and chromosomes have been stained with DAPI (Fig. 17). After counting chromosomes from 50 metaphase-spreads each, the results show that a significant number of E1KD and NMuMG-Cdc27 cells exhibited aneuploid chromosome numbers compared to NMuMG cells ($P<0.05$) (Fig. 17, graph). Knockdown of Cdc27 in E1KD-shCdc27 cells resulted in a decrease in aneuploidy compared to E1KD cells, supporting the hypothesis that Cdc27 is contributing directly to chromosomal stability in NMuMG cells (Fig. 17, graph). This data suggests that Cdc27 expression is directly related to chromosomal instability, and thus aneuploidy in mouse mammary epithelial cells.

To study the process through which cells transition from normal to highly metastatic, we generated a progression series of cell lines by *in vivo* passage of E1KD cells in NOD/SCID female mice. Cells that tended to metastasize to the lungs following orthotopic injection of cells into the mammary fat pad were isolated and cultured, then re-injected into mammary fat pads of NOD/SCID female mice. This allowed for the generation of a series of 3 cell lines in addition to NMuMG and E1KD, termed M1P, L1P, and L1P. Figure 18 contains the model depicting the way in which M1P, L1P, and L2P cells were

generated. These cell lines would then be analyzed for changes in gene expression, in an effort to decipher which biological pathways are exploited by metastatic cancer cells. Because the cell lines originated from an identical clone (E1KD), any genetic changes acquired are presumed to be a result of the selective pressures of the microenvironments encountered *in vivo*. Others have used a similar method of *in vivo* selection of cancer cells to generate cell lines with organ-specific metastatic tendencies (Bos et al., 2009; Minn et al., 2005).

The M1P, L1P, and L2P cell lines were characterized to assess their migratory and invasive capabilities compared to NMuMGs and E1KDs. L1P and L2P cells were both more migratory (Fig. 19A) and invasive (Fig. 19B) *in vitro* than E1KD and M1P cells, suggesting that cells with increased migratory and invasive phenotype are more likely to metastasize to the lung. The ability of cells to colonize lung tissue was assessed by tail-vein injection of E1KD, L1P, and L2P cells. We hypothesized that, given the same amount of time to colonize a secondary microenvironment, the more migratory and invasive cells would exhibit an enhanced ability to form metastatic outgrowths. Although tail-vein injection does not replicate all steps of metastasis, it is a widely-used practice to assess colonization potential (Elkin & Vlodavsky, 2001). Moreover, the ability of E1KD cells to undergo all steps of metastatic progression had been established, as L1P cells were isolated from E1KD cells that had invaded the basement membrane, intravasated, survived in the circulation, and extravasated in the lungs of mice. Immunohistological analysis of lungs of E1KD, L1P, and L2P-injected mice reveal that metastatic outgrowth is highest in L2P, followed by L1P and E1KD (Fig. 19C). This suggests that the L2P cells, in addition to being the most migratory and invasive, also exhibit the best ability to extravasate and colonize lung tissue.

Validation of the identity of M1P, L1P, and L2P cells was performed to ensure that they indeed originated as E1KD cells. Semi-quantitative RT-PCR analysis was performed on total RNA isolated from the cultured cells with gene specific primers to the *pSilencer* plasmid (Fig. 20). E1KD cells contain the *pSilencer* plasmid, encoding for an shRNA targeting hnRNP E1, and NMuMG cells do not. The presence of *pSilencer* gene in E1KD, M1P, L1P, and L2P, but not NMuMG, provides evidence that the progression series cells isolated from primary tumor and lung metastases were originally E1KD cells prior to *in vivo* passaging. RT-PCR analysis was also performed using gene specific primers for *Cdc27*, *Fzr1*, and *GAPDH* (control) (Fig. 20). The level of *Cdc27* mRNA is slightly increased in L1P and L2P cells, whereas the decrease in *Fzr1* mRNA is more obvious (Fig. 20). This data provides evidence that the loss of expression of *Fzr1* is an adaptation acquired by metastatic cells, and may play an important role in metastatic progression. The modest increase in *Cdc27* expression may be explained by the fact that the M1P, L1P, and L2P cells originated as E1KD cells, where we have shown that Cdc27 protein expression is increased post-transcriptionally as a result of loss of hnRNP E1 binding. Without hnRNP E1, a further increase in Cdc27 expression could be achieved by transcriptional up-regulation. Immunoblot analysis of whole cell lysates isolated from the progression series cell lines revealed a slight increase in Cdc27 expression and a large decrease in Cdh1 expression in the more metastatic cell lines. This data further supports the hypothesis that high Cdc27 and low Cdh1 expression correlate with metastatic potential in mouse mammary epithelial cells.

Cell cycle profile analysis was performed to analyze the distribution of cell populations throughout the cell cycle in M1P, L1P, and L2P cells. As mentioned previously,

loss of Cdh1 expression has been shown to result in decreased G1 populations (Sigl et al., 2009) and increased G2/M arrest (Engelbert et al., 2008; Garcia-Higuera et al., 2008). L1P and L2P cells had both larger G2/M populations and smaller G1 populations compared to NMuMG, E1KD, and M1P cell lines, suggesting premature S phase entry and mitotic arrest (Fig. 21, left). Metaphase spreads prepared from M1P, L1P, and L2P cells were analyzed and average chromosome counts indicate that L1P and L2P cells exhibited higher rates of aneuploidy than E1KD or M1P cells, suggesting that increased metastatic potential is linked to chromosomal instability (Fig, 21, right). In the future, knockdown of Cdc27 in L2P cells will be performed, followed by tail-vein injection of L2P or L2P-shCdc27 cells. The goal of this study will be to assess the impact of Cdc27 in regulating metastatic outgrowth. To this point, our data supports the hypothesis that Cdc27 directly influences chromosomal stability. We hypothesize that, by reducing expression of Cdc27 in L2P cells, their levels of chromosomal instability will be reduced, decreasing adaptability in changing microenvironments and so their metastatic potential will be attenuated.

Next, we were interested in determining whether these results translated to human disease. Since NMuMG cells are a normal mouse mammary gland cell line, we were interested in investigating the contribution of Cdc27 to human breast cancer. We analyzed several breast cancer cell lines for Cdc27 expression as well as cell cycle distribution and aneuploidy. The HMLE cell line was utilized, as it is a normal human mammary cell line comprised of two separate subpopulations: an epithelial-like subpopulation (HMLE-epithelial) that exhibits characteristics of differentiated epithelial cells, and a mesenchymal-like subpopulation (HMLE-mesenchymal) that exhibits some stem-like properties that have been implicated in metastatic progression (Mani et al., 2008). HnRNP

E1 was also stably knocked down by lentiviral transduction of shRNA in HMLE-epithelial cells in the laboratory and named HMLE-E1KD cells. MCF-7, MDA-MB-231, MDA-MB-468, T47D, and BT20 breast cancer cell lines were also assayed for Cdc27 expression. Immunoblot analysis revealed an increase in Cdc27 expression in the HMLE-mesenchymal and HMLE-E1KD cells compared to their epithelial counterpart, as well as high expression in MCF-7 and MDA-MB-231 breast cancer cell lines (Fig. 22). Unfortunately, this increased expression of Cdc27 did not consistently inversely correlate with expression of Cdh1 in the breast cancer cell lines, suggesting that the mechanisms regulating Cdh1 degradation previously supported by studies performed in NMuMG cells is more complex in human cells. GAPDH was included as a loading control (Fig. 22).

Flow cytometric analysis of the breast cancer cell lines revealed a decreased G1 phase in the same cell lines that exhibited highest expression of Cdc27 (Fig. 23). This data implies that high Cdc27 may be involved in premature S phase entry, a consequence of aberrant APC/C function. Furthermore, the cell line with the highest expression of Cdc27, MDA-MB-231 cells, exhibited the largest percentage of cells in G2/M (Fig. 23). Confocal microscopy of mitoses of MDA-MB-231 cells, as well as MCF-7 cells, would provide interesting evidence to support the correlation between high Cdc27 and the incidence of mitotic aberrations.

Many breast cancer cell lines exhibit polyploid chromosome numbers, and we were interested in determining whether the level of Cdc27 expression correlated with increased aneuploidy. Aneuploidy in normal cells results in cell cycle arrest and eventual DNA damage repair or cell death, however cancer cells exploit their increased susceptibility to chromosomal instability. Tumor cells experiencing a gain in copies of tumor promoting

genes and loss of tumor suppressor genes have a selective advantage, and so proliferate and progress. Furthermore, the ability to adapt to new microenvironments is facilitated by chromosomal instability (Hanahan & Weinberg, 2000, 2011). Metaphase spreads were prepared from breast cancer cell lines and 35 metaphases each were counted. HMLE-epithelial cells were nearly all diploid, with 46 chromosomes apiece, while HMLE-mesenchymal cells consistently exhibited a loss of one or two chromosomes (Fig. 24), similar to HMLE-E1KD cells. These results indicate that cells with a more invasive, metastatic phenotype are susceptible to increased variability in chromosome number. The difference in average chromosome number between HMLE-epithelial and HMLE-mesenchymal cells was significant ($P < 0.05$). MCF-7, BT20, and T47D cell lines all had chromosome numbers around 3n, while MDA-MB-231 and MDA-MB-468 cells had chromosome numbers over 2n (Fig. 24, graph). There was not an obvious relationship between the level of expression of Cdc27 and polyploidy among the breast cancer cell lines, however polyploidy was prevalent in the cell lines with the highest Cdc27 expression (MCF-7, MDA-MB-231, and T47D). The relationship between Cdc27 expression and chromosomal instability is not clear at this point in human cells, however the flow cytometry results suggest that there may be a relationship between Cdc27 and cell cycle progression in breast cancer cell lines. Knockdown studies would provide further clues as to the contribution of Cdc27 to the polyploidy observed in these cell lines.

Finally, breast cancer patient samples were acquired to assess Cdc27 expression in normal versus tumor tissue. Tissue microarray analysis of Cdc27 expression in 32 matched patient samples revealed that Cdc27 expression is increased significantly in tumor samples compared to normal breast tissue ($P < 0.001$) (Fig. 25A). Tumor tissue staining was then

scored to assign a “high” or “low” value to samples (Fig. 25B), and patient survival data was analyzed for correlation between staining score and recurrence. High Cdc27 staining predicted poor metastasis-free survival in breast cancer patients compared to low Cdc27 staining (Fig. 25B) (Log rank P <0.05). Cdc27 has not been shown previously to be a biomarker for poor prognosis in breast cancer, but our results indicate that increased Cdc27 expression in tumors could predict metastasis. We suggest that this is because increased Cdc27 expression is driving cell cycle progression in the presence of a damaged or aneuploid genome, and this increased susceptibility to chromosomal instability allows for cells to adapt to variable microenvironments during the process of metastasis.

The contribution of Cdh1 degradation in human breast cancer is not clear, as the pattern expression of Cdh1 was similar to that of Cdc27 in tissue microarray patient tumor samples. Cdh1 staining was significantly higher in tumor samples compared to normal tissue (P < 0.001) (Fig. 26). This data suggests that, while expression of Cdc27 significantly predicts metastatic recurrence in breast cancer, it does not appear to correlate with reduction of Cdh1 in the primary tumor. However, in tumor lymph node samples, 5 out of 6 of those with low Cdh1 score experienced disease recurrence, while only 2 out of 8 of those with high Cdh1 score experienced recurrence (Fig. 27A, B; Table 4). This suggests that Cdh1 may yet play a role in the metastatic progression of breast cancer, and its significance will be clearer in a larger sample size. The availability of metastatic lymph node tissue presents a unique advantage over studying cancer cell lines *in vitro* in that the expression levels of proteins can be obtained during distinct stages of disease progression for comparison. Furthermore, maintaining cell lines in culture over several passages does not accurately imitate the condition that cells face *in vivo.* For this reason, we submit that the

data obtained from breast cancer patients holds more clinical relevance than that of the cancer cell lines.

VI. Chapter 6: Conclusions

The results of this study lead us to conclude that the RNA-binding protein, hnRNP E1, regulates translation of mRNAs involved in biological processes besides epithelial-to-mesenchymal transition. HnRNP E1 is responsible for regulation of Cdc27 expression at the translational level, as is evidenced by assessment of total mRNA, protein, and polysome profiling of Cdc27 expression. Cdc27 translation is regulated in a cell cycle-dependent manner, increasing at the protein level shortly after the G1/S transition, but not at the transcript level. We identify Pak1 as the kinase responsible for phosphorylation of hnRNP E1 at threonine 60 and threonine 127 *in vitro*. The Pak1-specific inhibitor, IPA-3, prevents the translation of Cdc27 in the presence of hnRNP E1. In the absence of hnRNP E1, Cdc27 is constitutively expressed. Furthermore, IPA-3 prevents the phosphorylation of hnRNP E1 *in vivo*. Phospho-mutant GST-hnRNP E1 is not phosphorylated by Pak1 *in vitro*, further supporting the finding that T60 and T127 are the Pak1-specific phosphorylation sites. The role of hnRNP E1 in translational repression of mRNAs involved in several biological pathways indicates that it acts as a master regulator of cellular homeostasis.

The consequences of silencing hnRNP expression or constitutive Cdc27 expression include a decrease in the level of APC/C cofactor, Cdh1. Previously, we have shown that loss of Cdh1 expression results in stabilization of APC/C^{Cdh1} substrates and destabilization of APC/C^{Cdc20} substrates. The next step in assessing the role of Cdc27 in APC/C activity would be to interrogate APC/C substrates in the NMuMG-Cdc27 cell line. We predict that, due to the observed loss of Cdh1 expression, APC/C^{Cdh1} substrates will be stable in these cells. Inhibition of the proteasome using MG132 rescues Cdh1 levels in E1KDs, suggesting that proteasomal degradation is responsible for decreased levels observed in E1KD cells. We

show that the mitotic APC/C is constitutively active in E1KD cells, and that it is capable of ubiquitinating recombinant GST-Cdh1 *in vitro*. We show that overexpression of Flag-tagged Cdc27 alone is sufficient to cause a decrease in Cdh1 expression. Further studies are necessary to elucidate the mechanism responsible for Cdc27-mediated Cdh1 degradation.

Silencing expression of Cdc27 in E1KD cells results in a lower percentage of cells present in mitosis, suggesting a decrease in G2/M arrest that is observed in E1KD and NMuMG-Cdc27 cells. Since modulating Cdc27 expression impacts the distribution of cells in the cell cycle, a direct role for Cdc27 in regulating cell cycle is inferred. Immunofluorescent confocal microscopy of E1KD-shCdc27 cells is necessary to further investigate this claim. Mitotic aberrations are evidenced by immunofluorescent confocal microscopy in E1KD and NMuMG-Cdc27 cells, suggesting the direct role of increased Cdc27 expression in the deregulation of mitosis.

Analysis of the E1KD progression series of cells concluded that more invasive cells express moderately higher amounts of Cdc27 protein, while expressing substantially lower amounts of Cdh1 protein. These changes in expression are reflected at the transcriptional level, suggesting that they are the result of genetic changes experienced by cells as they face selective pressures *in vivo*. The more invasive cells also exhibit higher rates of aneuploidy, suggesting that chromosomal instability is an adaptation that evolves as a result of *in vivo* selection. Future studies will include knockdown of Cdc27 expression in the L2P cell line to assay metastatic potential *in vitro* and *in vivo*.

Studies in human breast cancer cell lines revealed that Cdc27 expression did not consistently inversely correlate with Cdh1 expression. Cdc27 expression was lowest in the most epithelial-like breast cancer cell lines, while Cdh1 was highest in these, suggesting

that their expression levels may play a role in the maintenance of epithelial phenotype. High Cdc27 expression in breast cancer cell lines positively correlated with mitotic index. In 3 of 5 breast cancer cell lines, aneuploidy positively correlated with expression of Cdc27. These results suggested a correlation between high Cdc27 expression and chromosomal instability.

Finally, tissue microarray analysis reveals significantly higher expression of Cdc27 in breast cancer patient tumor samples compared to normal tissue. Kaplan Meier survival analysis reveals that high expression of Cdc27 significantly predicts disease recurrence. While Cdh1 expression in tumors remained high, expression in tumor lymph nodes of patients experiencing disease recurrence was low in 5 of 6 patients. This data suggests that Cdc27 expression may represent a novel biomarker that predicts patient prognosis. The data also suggests that more aggressive cases of breast cancer may correlate with a loss of Cdh1 expression. In the future, I intend to expand the tissue microarray analysis to encompass a larger number of patient samples, as well as other cancer types. In doing so, we may find a relationship between metastatic propensity and Cdh1 expression.

References

Anderhub, S. J., Kramer, A., & Maier, B. (2012). Centrosome amplification in tumorigenesis. *Cancer Lett, 322*(1), 8-17. doi:10.1016/j.canlet.2012.02.006

Baker, K. E., & Coller, J. (2006). The many routes to regulating mRNA translation. *Genome Biol, 7*(12), 332. doi:10.1186/gb-2006-7-12-332

Bakhoum, S. F., & Compton, D. A. (2012). Chromosomal instability and cancer: a complex relationship with therapeutic potential. *J Clin Invest, 122*(4), 1138-1143. doi:10.1172/JCI59954

Balic, M., Lin, H., Young, L., Hawes, D., Giuliano, A., McNamara, G., . . . Cote, R. J. (2006). Most early disseminated cancer cells detected in bone marrow of breast cancer patients have a putative breast cancer stem cell phenotype. *Clin Cancer Res, 12*(19), 5615-5621. doi:10.1158/1078-0432.CCR-06-0169

Benmaamar, R., & Pagano, M. (2005). Involvement of the SCF complex in the control of Cdh1 degradation in S-phase. *Cell Cycle, 4*(9), 1230-1232. Retrieved from http://www.ncbi.nlm.nih.gov/pubmed/16123585

Bharadwaj, R., & Yu, H. (2004). The spindle checkpoint, aneuploidy, and cancer. *Oncogene, 23*(11), 2016-2027. doi:10.1038/sj.onc.1207374

Bos, P. D., Zhang, X. H., Nadal, C., Shu, W., Gomis, R. R., Nguyen, D. X., . . . Massague, J. (2009). Genes that mediate breast cancer metastasis to the brain. *Nature, 459*(7249), 1005-1009. doi:10.1038/nature08021

Brito, D. A., & Rieder, C. L. (2006). Mitotic checkpoint slippage in humans occurs via cyclin B destruction in the presence of an active checkpoint. *Curr Biol, 16*(12), 1194-1200. doi:10.1016/j.cub.2006.04.043

Chaudhury, A., Chander, P., & Howe, P. H. (2010). Heterogeneous nuclear ribonucleoproteins (hnRNPs) in cellular processes: Focus on hnRNP E1's multifunctional regulatory roles. *RNA, 16*(8), 1449-1462. doi:10.1261/rna.2254110

Chaudhury, A., Hussey, G. S., Ray, P. S., Jin, G., Fox, P. L., & Howe, P. H. (2010). TGF-beta-mediated phosphorylation of hnRNP E1 induces EMT via transcript-selective translational induction of Dab2 and ILEI. *Nat Cell Biol, 12*(3), 286-293. doi:10.1038/ncb2029

Chu, I. M., Hengst, L., & Slingerland, J. M. (2008). The Cdk inhibitor p27 in human cancer: prognostic potential and relevance to anticancer therapy. *Nat Rev Cancer, 8*(4), 253-267. doi:10.1038/nrc2347

Clijsters, L., Ogink, J., & Wolthuis, R. (2013). The spindle checkpoint, APC/C(Cdc20), and APC/C(Cdh1) play distinct roles in connecting mitosis to S phase. *J Cell Biol, 201*(7), 1013-1026. doi:10.1083/jcb.201211019

Deacon, S. W., Beeser, A., Fukui, J. A., Rennefahrt, U. E., Myers, C., Chernoff, J., & Peterson, J. R. (2008). An isoform-selective, small-molecule inhibitor targets the autoregulatory mechanism of p21-activated kinase. *Chem Biol, 15*(4), 322-331. doi:10.1016/j.chembiol.2008.03.005

Dean, P. N., & Jett, J. H. (1974). Mathematical analysis of DNA distributions derived from flow microfluorometry. *J Cell Biol, 60*(2), 523-527. Retrieved from http://www.ncbi.nlm.nih.gov/pubmed/4855906

Dennis, G., Jr., Sherman, B. T., Hosack, D. A., Yang, J., Gao, W., Lane, H. C., & Lempicki, R. A. (2003). DAVID: Database for Annotation, Visualization, and Integrated Discovery.

Genome Biol, 4(5), P3. Retrieved from http://www.ncbi.nlm.nih.gov/pubmed/12734009

Dreyfuss, G., Matunis, M. J., Pinol-Roma, S., & Burd, C. G. (1993). hnRNP proteins and the biogenesis of mRNA. *Annu Rev Biochem, 62*, 289-321. doi:10.1146/annurev.bi.62.070193.001445

Dumont, N., Liu, B., Defilippis, R. A., Chang, H., Rabban, J. T., Karnezis, A. N., . . . Tlsty, T. D. (2013). Breast fibroblasts modulate early dissemination, tumorigenesis, and metastasis through alteration of extracellular matrix characteristics. *Neoplasia, 15*(3), 249-262. Retrieved from http://www.ncbi.nlm.nih.gov/pubmed/23479504

Elkin, M., & Vlodavsky, I. (2001). Tail vein assay of cancer metastasis. *Curr Protoc Cell Biol, Chapter 19*, Unit 19 12. doi:10.1002/0471143030.cb1902s12

Engelbert, D., Schnerch, D., Baumgarten, A., & Wasch, R. (2008). The ubiquitin ligase APC(Cdh1) is required to maintain genome integrity in primary human cells. *Oncogene, 27*(7), 907-917. doi:10.1038/sj.onc.1210703

Eytan, E., Sitry-Shevah, D., Teichner, A., & Hershko, A. (2013). Roles of different pools of the mitotic checkpoint complex and the mechanisms of their disassembly. *Proc Natl Acad Sci U S A, 110*(26), 10568-10573. doi:10.1073/pnas.1308928110

Fukushima, H., Ogura, K., Wan, L., Lu, Y., Li, V., Gao, D., . . . Wei, W. (2013). SCF-mediated Cdh1 degradation defines a negative feedback system that coordinates cell-cycle progression. *Cell Rep, 4*(4), 803-816. doi:10.1016/j.celrep.2013.07.031

Garcia-Higuera, I., Manchado, E., Dubus, P., Canamero, M., Mendez, J., Moreno, S., & Malumbres, M. (2008). Genomic stability and tumour suppression by the APC/C cofactor Cdh1. *Nat Cell Biol, 10*(7), 802-811. doi:10.1038/ncb1742

Ghazalpour, A., Bennett, B., Petyuk, V. A., Orozco, L., Hagopian, R., Mungrue, I. N., . . . Lusis, A. J. (2011). Comparative analysis of proteome and transcriptome variation in mouse. *PLoS Genet, 7*(6), e1001393. doi:10.1371/journal.pgen.1001393

Hanahan, D., & Weinberg, R. A. (2000). The hallmarks of cancer. *Cell, 100*(1), 57-70. Retrieved from http://www.ncbi.nlm.nih.gov/pubmed/10647931

Hanahan, D., & Weinberg, R. A. (2011). Hallmarks of cancer: the next generation. *Cell, 144*(5), 646-674. doi:10.1016/j.cell.2011.02.013

Harper, J. V. (2005). Synchronization of cell populations in G1/S and G2/M phases of the cell cycle. *Methods Mol Biol, 296*, 157-166. Retrieved from http://www.ncbi.nlm.nih.gov/pubmed/15576930

Heng, H. H., Bremer, S. W., Stevens, J. B., Horne, S. D., Liu, G., Abdallah, B. Y., . . . Ye, C. J. (2013). Chromosomal instability (CIN): what it is and why it is crucial to cancer evolution. *Cancer Metastasis Rev, 32*(3-4), 325-340. doi:10.1007/s10555-013-9427-7

Howley, B. V., Hussey, G. S., Link, L. A., & Howe, P. H. (2015). Translational regulation of inhibin betaA by TGFbeta via the RNA-binding protein hnRNP E1 enhances the invasiveness of epithelial-to-mesenchymal transitioned cells. *Oncogene*. doi:10.1038/onc.2015.238

Huang da, W., Sherman, B. T., & Lempicki, R. A. (2009). Systematic and integrative analysis of large gene lists using DAVID bioinformatics resources. *Nat Protoc, 4*(1), 44-57. doi:10.1038/nprot.2008.211

Huang, D. W., Sherman, B. T., & Lempicki, R. A. (2008). Systematic and integrative analysis of large gene lists using DAVID bioinformatics resources. *Nat. Protocols, 4*(1), 44-57.

doi:http://www.nature.com/nprot/journal/v4/n1/suppinfo/nprot.2008.211_S1.html

Huang, D. W., Sherman, B. T., & Lempicki, R. A. (2009). Bioinformatics enrichment tools: paths toward the comprehensive functional analysis of large gene lists. *Nucleic Acids Research, 37*(1), 1-13. doi:10.1093/nar/gkn923

Hussey, G. S., Chaudhury, A., Dawson, A. E., Lindner, D. J., Knudsen, C. R., Wilce, M. C., . . . Howe, P. H. (2011). Identification of an mRNP complex regulating tumorigenesis at the translational elongation step. *Mol Cell, 41*(4), 419-431. doi:10.1016/j.molcel.2011.02.003

Hussey, G. S., Link, L. A., Brown, A. S., Howley, B. V., Chaudhury, A., & Howe, P. H. (2012). Establishment of a TGFbeta-induced post-transcriptional EMT gene signature. *PLoS One, 7*(12), e52624. doi:10.1371/journal.pone.0052624

Izawa, D., & Pines, J. (2011). How APC/C-Cdc20 changes its substrate specificity in mitosis. *Nat Cell Biol, 13*(3), 223-233. doi:10.1038/ncb2165

Kramer, E. R., Scheuringer, N., Podtelejnikov, A. V., Mann, M., & Peters, J. M. (2000). Mitotic regulation of the APC activator proteins CDC20 and CDH1. *Mol Biol Cell, 11*(5), 1555-1569. Retrieved from http://www.ncbi.nlm.nih.gov/pubmed/10793135

Kronja, I., & Orr-Weaver, T. L. (2011). Translational regulation of the cell cycle: when, where, how and why? *Philos Trans R Soc Lond B Biol Sci, 366*(1584), 3638-3652. doi:10.1098/rstb.2011.0084

Kurland, J. F., & Tansey, W. P. (2004). Crashing waves of destruction: the cell cycle and APC(Cdh1) regulation of SCF(Skp2). *Cancer Cell, 5*(4), 305-306. Retrieved from http://www.ncbi.nlm.nih.gov/pubmed/15093536

Lee, D. H., & Goldberg, A. L. (1998). Proteasome inhibitors: valuable new tools for cell biologists. *Trends Cell Biol, 8*(10), 397-403. Retrieved from http://www.ncbi.nlm.nih.gov/pubmed/9789328

Listovsky, T., Oren, Y. S., Yudkovsky, Y., Mahbubani, H. M., Weiss, A. M., Lebendiker, M., & Brandeis, M. (2004). Mammalian Cdh1/Fzr mediates its own degradation. *EMBO J, 23*(7), 1619-1626. doi:10.1038/sj.emboj.7600149

Listovsky, T., & Sale, J. E. (2013). Sequestration of CDH1 by MAD2L2 prevents premature APC/C activation prior to anaphase onset. *J Cell Biol, 203*(1), 87-100. doi:10.1083/jcb.201302060

Mani, S. A., Guo, W., Liao, M. J., Eaton, E. N., Ayyanan, A., Zhou, A. Y., . . . Weinberg, R. A. (2008). The epithelial-mesenchymal transition generates cells with properties of stem cells. *Cell, 133*(4), 704-715. doi:10.1016/j.cell.2008.03.027

Maroto, B., Ye, M. B., von Lohneysen, K., Schnelzer, A., & Knaus, U. G. (2008). P21-activated kinase is required for mitotic progression and regulates Plk1. *Oncogene, 27*(36), 4900-4908. doi:10.1038/onc.2008.131

Martin, B. T., & Strebhardt, K. (2006). Polo-like kinase 1: target and regulator of transcriptional control. *Cell Cycle, 5*(24), 2881-2885. Retrieved from http://www.ncbi.nlm.nih.gov/pubmed/17172872

Meng, Q., Rayala, S. K., Gururaj, A. E., Talukder, A. H., O'Malley, B. W., & Kumar, R. (2007). Signaling-dependent and coordinated regulation of transcription, splicing, and translation resides in a single coregulator, PCBP1. *Proc Natl Acad Sci U S A, 104*(14), 5866-5871. doi:10.1073/pnas.0701065104

Merrick, W. C., & Hensold, J. O. (2001). Analysis of eukaryotic translation in purified and semipurified systems. *Curr Protoc Cell Biol, Chapter 11*, Unit 11 19. doi:10.1002/0471143030.cb1109s08

Minn, A. J., Gupta, G. P., Siegel, P. M., Bos, P. D., Shu, W., Giri, D. D., . . . Massague, J. (2005). Genes that mediate breast cancer metastasis to lung. *Nature, 436*(7050), 518-524. doi:10.1038/nature03799

Moller, M. B. (2000). P27 in cell cycle control and cancer. *Leuk Lymphoma, 39*(1-2), 19-27. doi:10.3109/10428190009053535

Morales, J., Russell, J. E., & Liebhaber, S. A. (1997). Destabilization of human alpha-globin mRNA by translation anti-termination is controlled during erythroid differentiation and is paralleled by phased shortening of the poly(A) tail. *J Biol Chem, 272*(10), 6607-6613. Retrieved from http://www.ncbi.nlm.nih.gov/pubmed/9045690

Moustakas, A., & Heldin, C. H. (2005). Non-Smad TGF-beta signals. *J Cell Sci, 118*(Pt 16), 3573-3584. doi:10.1242/jcs.02554

Nowak, M. A., Komarova, N. L., Sengupta, A., Jallepalli, P. V., Shih Ie, M., Vogelstein, B., & Lengauer, C. (2002). The role of chromosomal instability in tumor initiation. *Proc Natl Acad Sci U S A, 99*(25), 16226-16231. doi:10.1073/pnas.202617399

Ostareck, D. H., Ostareck-Lederer, A., Wilm, M., Thiele, B. J., Mann, M., & Hentze, M. W. (1997). mRNA silencing in erythroid differentiation: hnRNP K and hnRNP E1 regulate 15-lipoxygenase translation from the 3' end. *Cell, 89*(4), 597-606. Retrieved from http://www.ncbi.nlm.nih.gov/pubmed/9160751

Ostareck-Lederer, A., Ostareck, D. H., Cans, C., Neubauer, G., Bomsztyk, K., Superti-Furga, G., & Hentze, M. W. (2002). c-Src-mediated phosphorylation of hnRNP K drives

translational activation of specifically silenced mRNAs. *Mol Cell Biol, 22*(13), 4535-4543. Retrieved from http://www.ncbi.nlm.nih.gov/pubmed/12052863

Ostareck-Lederer, A., Ostareck, D. H., & Hentze, M. W. (1998). Cytoplasmic regulatory functions of the KH-domain proteins hnRNPs K and E1/E2. *Trends Biochem Sci, 23*(11), 409-411. Retrieved from http://www.ncbi.nlm.nih.gov/pubmed/9852755

Ostareck-Lederer, A., Ostareck, D. H., Standart, N., & Thiele, B. J. (1994). Translation of 15-lipoxygenase mRNA is inhibited by a protein that binds to a repeated sequence in the 3' untranslated region. *EMBO J, 13*(6), 1476-1481. Retrieved from http://www.ncbi.nlm.nih.gov/pubmed/8137829

Pawar, S. A., Sarkar, T. R., Balamurugan, K., Sharan, S., Wang, J., Zhang, Y., . . . Sterneck, E. (2010). C/EBP{delta} targets cyclin D1 for proteasome-mediated degradation via induction of CDC27/APC3 expression. *Proc Natl Acad Sci U S A, 107*(20), 9210-9215. doi:10.1073/pnas.0913813107

Penas, C., Ramachandran, V., & Ayad, N. G. (2011). The APC/C Ubiquitin Ligase: From Cell Biology to Tumorigenesis. *Front Oncol, 1*, 60. doi:10.3389/fonc.2011.00060

Peters, J. M. (2002). The anaphase-promoting complex: proteolysis in mitosis and beyond. *Mol Cell, 9*(5), 931-943. Retrieved from http://www.ncbi.nlm.nih.gov/pubmed/12049731

Peters, J. M. (2006). The anaphase promoting complex/cyclosome: a machine designed to destroy. *Nat Rev Mol Cell Biol, 7*(9), 644-656. doi:10.1038/nrm1988

Pfleger, C. M., & Kirschner, M. W. (2000). The KEN box: an APC recognition signal distinct from the D box targeted by Cdh1. *Genes Dev, 14*(6), 655-665. Retrieved from http://www.ncbi.nlm.nih.gov/pubmed/10733526

Prosser, S. L., Samant, M. D., Baxter, J. E., Morrison, C. G., & Fry, A. M. (2012). Oscillation of APC/C activity during cell cycle arrest promotes centrosome amplification. *J Cell Sci, 125*(Pt 22), 5353-5368. doi:10.1242/jcs.106096

Schwanhausser, B., Busse, D., Li, N., Dittmar, G., Schuchhardt, J., Wolf, J., . . . Selbach, M. (2011). Global quantification of mammalian gene expression control. *Nature, 473*(7347), 337-342. doi:10.1038/nature10098

Sigl, R., Wandke, C., Rauch, V., Kirk, J., Hunt, T., & Geley, S. (2009). Loss of the mammalian APC/C activator FZR1 shortens G1 and lengthens S phase but has little effect on exit from mitosis. *J Cell Sci, 122*(Pt 22), 4208-4217. doi:10.1242/jcs.054197

Silvera, D., Formenti, S. C., & Schneider, R. J. (2010). Translational control in cancer. *Nat Rev Cancer, 10*(4), 254-266. doi:10.1038/nrc2824

Sudakin, V., Chan, G. K., & Yen, T. J. (2001). Checkpoint inhibition of the APC/C in HeLa cells is mediated by a complex of BUBR1, BUB3, CDC20, and MAD2. *J Cell Biol, 154*(5), 925-936. doi:10.1083/jcb.200102093

Tipton, A. R., Wang, K., Link, L., Bellizzi, J. J., Huang, H., Yen, T., & Liu, S. T. (2011). BUBR1 and closed MAD2 (C-MAD2) interact directly to assemble a functional mitotic checkpoint complex. *J Biol Chem, 286*(24), 21173-21179. doi:10.1074/jbc.M111.238543

Viaud, J., & Peterson, J. R. (2009). An allosteric kinase inhibitor binds the p21-activated kinase autoregulatory domain covalently. *Mol Cancer Ther, 8*(9), 2559-2565. doi:10.1158/1535-7163.MCT-09-0102

Visintin, R., Prinz, S., & Amon, A. (1997). CDC20 and CDH1: a family of substrate-specific activators of APC-dependent proteolysis. *Science, 278*(5337), 460-463. Retrieved from http://www.ncbi.nlm.nih.gov/pubmed/9334304

Wang, R. A., Zhang, H., Balasenthil, S., Medina, D., & Kumar, R. (2006). PAK1 hyperactivation is sufficient for mammary gland tumor formation. *Oncogene, 25*(20), 2931-2936. doi:10.1038/sj.onc.1209309

Weaver, B. A., & Cleveland, D. W. (2006). Does aneuploidy cause cancer? *Curr Opin Cell Biol, 18*(6), 658-667. doi:10.1016/j.ceb.2006.10.002

Weiss, I. M., & Liebhaber, S. A. (1994). Erythroid cell-specific determinants of alpha-globin mRNA stability. *Mol Cell Biol, 14*(12), 8123-8132. Retrieved from http://www.ncbi.nlm.nih.gov/pubmed/7969150

Xia, M., He, H., Wang, Y., Liu, M., Zhou, T., Lin, M., . . . Sha, J. (2012). PCBP1 is required for maintenance of the transcriptionally silent state in fully grown mouse oocytes. *Cell Cycle, 11*(15), 2833-2842. doi:10.4161/cc.21169

Zavadil, J., & Bottinger, E. P. (2005). TGF-beta and epithelial-to-mesenchymal transitions. *Oncogene, 24*(37), 5764-5774. doi:10.1038/sj.onc.1208927

Zeng, X., & King, R. W. (2012). An APC/C inhibitor stabilizes cyclin B1 by prematurely terminating ubiquitination. *Nat Chem Biol, 8*(4), 383-392. doi:10.1038/nchembio.801

Zeng, X., Sigoillot, F., Gaur, S., Choi, S., Pfaff, K. L., Oh, D. C., . . . King, R. W. (2010). Pharmacologic inhibition of the anaphase-promoting complex induces a spindle checkpoint-dependent mitotic arrest in the absence of spindle damage. *Cancer Cell, 18*(4), 382-395. doi:10.1016/j.ccr.2010.08.010

Appendix A

Buffer Recipes

RIPA lysis buffer

50 mM Tris pH 8.0, 150 mM sodium chloride (NaCl), 1% v/v NP-40, 0.5% w/v sodium deoxycholate, 0.1% w/v sodium dodecyl sulfate (SDS)

Laemmli sample buffer

60 mM Tris-Cl pH 6.8, 2% w/v SDS, 0.01% w/v bromophenol blue, 5% v/v β-mercaptoethanol, 10% glycerol

Kinase assay lysis buffer

50 mM Tris pH 8.0, 150 mM NaCl, 10% glycerol, 1% Tween-20, 1 mM sodium fluoride (NaF), 1 mM sodium orthovanadate (Na_3VO_4), 1 mM dithiothretiol (DTT), 50 mM β-glycerophosphate

Kinase reaction buffer

10 mM HEPES pH 7.5, 50 mM NaCl, 10 mM $MgCl_2$, 1 mM DTT, 50 mM β-glycerophosphate

Tris-buffered saline with Tween-20 (TBS-T)

20 mM Tris pH 7.6, 150 mM NaCl, 0.1% Tween-20

S100 lysis buffer

20 mM Tris pH 7.4, 10 mM KCl, 1.5 mM $MgCl_2$, 1 mM ethylene glycol tetraacetic acid (EGTA), 1 mM ethylenediaminetetraacetic acid (EDTA), 1 mM DTT, protease inhibitors

In vitro ubiquitination lysis buffer

1X Phosphate buffered saline, 1% v/v NP-40, 0.5% v/v glycerol

Ubiquitination reaction buffer

10 mM Tris-Cl pH 7.6, 5 mM magnesium chloride, 10 mM dithiothreitol, 1 mg/ml human recombinant ubiquitin, 10 mM phosphocreatine, 50 μg/ml creatine phosphokinase, 15 mM adenosine triphosphate, 0.15 mg/ml bovine serum albumin